Response of phytoplankton communities to the onset of the 2020 summer marine heatwave in the Drake Passage and Antarctic Peninsula.

- Andrés S. Rigual-Hernández^{1,*}, Amy Leventer², Manuel Fernández-Barba³, José A. Flores¹, Gabriel Navarro³, Johan Etourneau⁴, Dimitris Evangelinos^{5,6}, Megan Duffy², Carlota Escutia⁷,
- Fernando Bohoyo⁸, José M. Sánchez-Santos⁹, Manon Sabourdy^{4,10}, Francisco J. Jiménez-
- 6 Espejo⁷, and María A. Bárcena ¹
 - 1. Área de Paleontología, Departamento de Geología, Universidad de Salamanca, 37008 Salamanca, Spain
 - 2. Department of Geology, Colgate University, Hamilton, NY, USA.
- Department of Ecology and Coastal Management, Institute of Marine Sciences of
 Andalusia (ICMAN), Spanish National Research Council (CSIC), 11519 Puerto Real,
 Cádiz, Spain.
- 4. University of Bordeaux, CNRS, Bordeaux INP, EPOC, UMR 5805, Pessac, France.
- 5. GRC Geociències Marines, Departament de Dinàmica de la Terra i de l'Oceà, Universitat
 de Barcelona, Barcelona, Spain.
- 16 6. Department of Earth Science and Engineering, Imperial College London, London, UK.
 - 7. Instituto Andaluz de Ciencias de la Tierra (IACT-CSIC), Armilla, Spain.
 - 8. Instituto Geológico y Minero de España (IGME-CSIC), Madrid, Spain.
 - 9. Departamento de Estadística, Universidad de Salamanca, 37008 Salamanca, Spain
- 10. Laboratoire des Sciences du Climat et de l'Environnement, LSCE/IPSL, UMR CEA-CNRS UVSQ 8212 CEA Saclay, Gif sur Yvette
- 22 * Corresponding author. E-mail address: arigual@usal.es (A. S. Rigual-Hernández).

23 Abstract

7

8

9

17

18

19

24 Extreme warming events are increasingly more intense and frequent in the global ocean. These 25 events are predicted to drive profound and widespread effects on marine ecosystems, yet their 26 impact on phytoplankton, the base of the marine food web, is still largely unknown. Our 27 understanding of the impact of these phenomena in marine ecosystems is particularly poor in 28 the remote and logistically challenging Southern Ocean. During summer 2020, the research 29 vessel Hespérides sampled the water column of the Drake Passage and northern Antarctic 30 Peninsula before (early January) and during the early phase (late January-early February) of a 31 Marine Heat Wave (MHW), that resulted in sea surface temperature anomalies of up to +3°C. 32 Here, we take advantage of this exceptional opportunity to document the effects of an extreme 33 warming event on the nutrient and phytoplankton (diatom and coccolithophores) distributions 34 across the main zonal systems of the Southern Ocean. Overall, our results indicate that 35 biogeographical variability of diatom and coccolithophore assemblages, the two dominant 36 phytoplankton groups in the Southern Ocean, mirrored the physical and chemical properties of 37 the water masses delineated by the Southern Ocean fronts before and during the onset of the 38 marine heat wave. Analysis of a suite of satellite-derived oceanographic parameters revealed 39 that development and persistence of the 2020 marine heat wave were closely tied to mesoscale 40 anticyclonic eddy dynamics. The increase in sea surface temperatures during the onset of the 41 marine heat wave was associated with a remarkable increase in diatom abundance reaching 42 bloom concentrations and a shift in the diatom assemblage towards an increase in the relative 43 abundance of the small diatom Fragilariopsis cylindrus/nana in the southern Drake Passage. 44 Notably, the diatom bloom was not coupled with a statistically significant change in chlorophyll-45 a, as derived from in-situ fluorescence, or modelled Net Primary Production. It is likely that the

differing contribution of other phytoplankton groups and/or a shift in the average phytoplankton size before and during the MHW might be responsible for these results. Average coccolithophore abundance was lower than previous studies in the Drake Passage and decreased during the MHW. We speculate that the remarkable nitrate decrease by approximately one order of magnitude lower than average summer concentrations might have been responsible for the reduction in coccolithophore numbers. Low nitrate levels are attributed to either the advection of nitrate poor waters from lower latitudes by an anticyclonic eddy and/or nutrient consumption by substantial development of soft-tissue phytoplankton biomass. Overall, our results reinforce the notion that a warmer Southern Ocean will favour an increase of small phytoplankton cells in the southern Drake Passage and northern Antarctic Peninsula with unpredictable consequences in the marine-food web and biogeochemical cycles that need to be urgently quantified and parametrized.

1. Introduction

The global ocean is warming at an unprecedented rapid rate, with modern global sea surface temperatures being nearly 1°C higher than 1850–1900 as a result of anthropogenic climate change (Lee et al., 2023). One consequence of this temperature rise is the increased likelihood of Marine Heat Waves (MHWs; Holbrook et al., 2019) which can be broadly defined as periods of anomalously high warm water temperatures that may last up to several months and may cover thousands of square kilometres (Oliver et al., 2021). These extreme warm ocean temperature events can lead to substantial and diverse impacts on marine ecosystems, such as, (i) global-scale coral bleaching events (Eakin et al., 2019), (ii) profound changes in diversity and structure of marine ecosystems (Wernberg et al., 2013; Wernberg et al., 2016; Garrabou et al., 2022), (iii) reduction of carbon sequestration (Gao et al., 2021), (iv) shifts in the geographical distributions of zooplankton and (v) mass mortalities of mammals and birds (Bond et al., 2015; Cavole et al., 2016; Hobday et al., 2018). However, little information exists about the effects of MHW on phytoplankton in the Southern Ocean, which represents the base of its marine food webs and regulates its biogeochemical cycles.

The Antarctic Peninsula (AP) is one of the fastest warming regions in the world's oceans (Vaughan et al., 2003; Jones et al., 2019; Gorodetskaya et al., 2023) and is experiencing an increase in the frequency of extreme warming events both in the atmosphere (Turner et al., 2021) and in the ocean (Montie et al., 2020). The increase in air and sea surface temperatures are shortening the sea ice season and driving the retreat of glaciers at an increasingly accelerating rate (Cook et al., 2005; Eayrs et al., 2019; Blanchard-Wrigglesworth et al., 2021; Suryawanshi et al., 2023; Davison et al., 2024). The enhanced influx of fresh waters in coastal waters due to ice melting results in a strengthening of the stratification of the water column, while the increase of lithogenic particles - derived from subglacial erosion - increases turbidity and enriches the surface ocean with nutrients (Meredith et al., 2018). The abundance, structure and function of phytoplankton communities in the AP are experiencing changes driven by this rapid environmental change. Primary production has increased in the Western Antarctic Peninsula (WAP) during the last two decades (1998 to 2022), mainly due to the decline in sea ice coverage that results in longer blooms (Ferreira et al., 2024; Isla et al., 2025). As summarized in the comprehensive review by Deppeler and Davidson (2017), changes in the makeup of AP phytoplankton communities could also have profound effects in the local food chain (Ballerini et al., 2014). Freshening of surface waters is expected to drive a shift from diatom-dominated communities to cryptophytes and small flagellates (Moline et al., 2004; Montes-Hugo et al., 2008). This shift in the dominance is thought to be driven by the higher physiological tolerance

of cryptophytes to lower salinity waters associated with melt-water events (see Moline et al., 2004 and references therein). Since krill feed mainly of phytoplankton cells larger than 10 μ m, the overall size reduction of phytoplankton communities has resulted in a decrease of krill numbers and an increase in salp abundance (grazers unaffected by the size of their prey) (Moline et al., 2004; Moline et al., 2008; Plum et al., 2020; Pauli et al., 2021). Since salps are not a preferred food source for some of the major macrofaunal groups of the AP, such as penguins and seals, changes in the composition of phytoplankton populations towards smaller and non-siliceous phytoplankton are anticipated to have detrimental effects in the whole ecosystem.

Moreover, the climate-induced changes in phytoplankton communities are likely to alter the functioning of biogeochemical cycles in the AP, particularly the carbon cycle through impacts in the biological pump. On the one hand, ice loss results (i) in the fertilization of the surface ocean with nutrients fuelling phytoplankton blooms in areas previously covered by ice and in wake of icebergs (Bertolin and Schloss, 2009; Vernet et al., 2012) and (ii) in the creation of new carbon sinks in open ocean environments (Peck et al., 2010). On the other hand, the abovementioned shift in dominance from diatoms to cryptophytes will most likely result in a less efficient biological pump. This is because the organic content of particles lacking mineral ballast (such as cryptophytes) remineralizes at shallower depths than those associated with biominerals such as opal produced by diatoms. Moreover, while diatoms form fast-sinking algal aggregates and are an important component of faecal pellets produced by zooplankton (Green et al., 1998; Smetacek et al., 2004), cryptophytes are not grazed efficiently by Antarctic krill which most likely results in a weaker carbon pump. The net effect of all above mentioned changes over the AP marine ecosystems and their biogeochemical cycles is yet to be determined.

Notably, despite a growing body of evidence that supports the major influence of climate change and its cascading impacts on AP ecosystems (Plum et al., 2020; Oh et al., 2022; Thomalla et al., 2023; Ferreira et al., 2024), very limited scientific studies have addressed the effects of short-term climate extremes (such as MHWs) on phytoplankton primary productivity (Fernández-Barba et al., 2024) and its composition (Antoni et al., 2020). This information is particularly important because temperature is one of the main factors controlling phytoplankton growth by directly influencing metabolic rates (Eppley, 1972). One of the few field-based evidence studies addressing this point is the work by Latorre et al. (2023) who documented changes in the biomass of most plankton species in relation to an atmospheric heatwave in a cove of King George Island, South Shetlands. However, the effects of the local scale forcing in this small inlet make the extrapolation of their results to pelagic environments of the AP and Drake Passage difficult. Results of a near-global ocean physical-biogeochemical model indicate that background nutrient conditions most likely represents a major control in determining the impact of heatwaves on phytoplankton productivity (Hayashida et al., 2020). While in nutrient-poor regions marine heatwaves generally will result in weaker phytoplankton blooms, in nutrient-rich waters the heatwave blooms are predicted to result in higher phytoplankton numbers. Based on this notion, phytoplankton growth in the nutrient-rich waters of the AP will be most likely stimulated by marine heatwaves. Since the frequency and intensity of MHWs are expected to substantially increase in the coming decades (Frölicher et al., 2018; Oliver et al., 2018; Oliver et al., 2021), it is of critical importance to evaluate their impacts on Southern Ocean marine ecosystems.

Here we report on data of major phytoplankton groups (diatoms and coccolithophores), fluorescence (as an indicator of algal biomass accumulation), net primary production, nutrients (silicate, nitrate and phosphate) and Sea Surface Temperatures (SST) measured before and

during the onset of a marine heatwave that affected the Drake Passage during January and February 2020. Moreover, we characterize the drivers of the warm water anomaly registered during the northbound transit using satellite-derived and reanalysis data. Our study builds on previous findings (Moline et al., 2004; Montes-Hugo et al., 2008) showing long-term warming and shifts toward smaller phytoplankton cells in Antarctic waters. The combination of *in-situ* measurements with satellite-derived environmental parameters allowed us to specifically test the hypothesis that marine heatwaves act as acute perturbations capable of accelerating such community shifts. Given the projected increase in MHW frequency, understanding these short-term biological responses is critical to parameterizing their effects on Antarctic marine food webs and biogeochemical cycles.

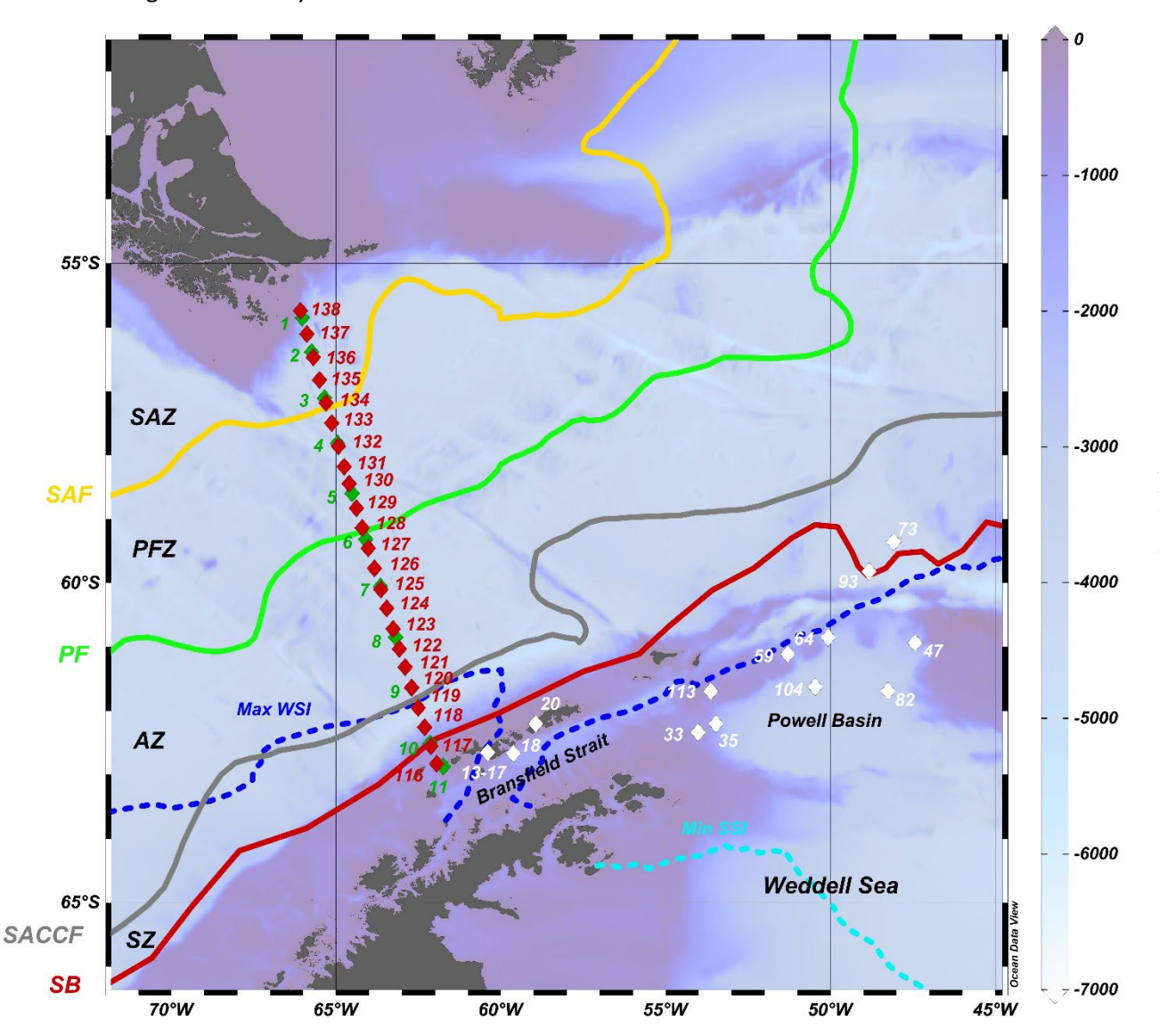


Figure 1. Bathymetric map showing the sampling locations during the POWELL-2020 campaign in the Drake Passage and northern Antarctic Peninsula. Green and red diamonds represent stations sampled during the southbound (4th to 5th of January 2020) and northound (31st January to 2nd February 2020) transits, respectively, while white dots depict representative stations from the Bransfield Strait and northern Weddell Sea (including the Powell Basin) analyzed in this study. Abbreviations: SAZ – Subantarctic Zone, SAF – Subantarctic Front, PFZ – Polar Frontal Zone, PF – polar front, AZ – Antarctic zone, SACCF – Southern Antarctic Circumpolar Current Front, SZ – Southern Zone and SB – Southern Boundary, Max WSI – maximum winter sea ice extent and Min

SSI – minimum summer sea ice extent. Oceanic fronts after Orsi et al. (1995) and sea ice climatology for 1981 to 2010 after Fetterer et al. (2002, updated 2009). Ocean Data View software (Schlitzer, 2021) was used to generate this figure.

1.2 Oceanographic setting

The study region covered in the present work is the Drake Passage, the Bransfield Strait and the Powell Basin, extending approximately from 56°S to 64°S and 64°W to 47°W (Fig. 1). The Antarctic Circumpolar Current (ACC), the world's largest ocean current system, flows from west to east in the Drake Passage, connecting surface and deep layers of the ocean (Rintoul et al., 2018). The ACC consists of four major hydrographic fronts from north to south within the Drake Passage: the Subantarctic Zone (SAZ), the Subantarctic Front (SAF), the Southern Antarctic Circumpolar Front (SACCF) and the Southern Boundary front (Orsi et al., 1995; Rintoul et al., 2018). The Drake Passage is the narrowest constriction of the ACC, with a width of approximately 800 km. As a result, the ACC fronts are closely spaced in this region compared to other sectors of the Southern Ocean (Meredith et al., 2011). The position of the above-mentioned fronts exhibit temporal variations and are influenced by disturbances by mesoscale eddies and meanders (e.g. Rintoul et al., 1997; Rintoul and Sokolov, 2001). Both models and observations indicate the Drake Passage is one of the few key areas in the Southern Ocean where eddy heat transport across the ACC fronts is intensified (e.g. Gutierrez-Villanueva et al., 2020).

Phytoplankton growth in the Southern Ocean is controlled by multiple environmental factors, among which low light levels in deep wind-mixed surface layers and low concentrations of the micronutrient iron, stand out as the main factors controlling primary production (Martin et al., 1990; Boyd and Trull, 2007; Venables and Moore, 2010). The ACC carries Circumpolar Deep Water (CDW), the most widespread water mass in the Southern Ocean. Wind-driven upwelling of CDW south of the PF brings to the surface layer large amounts of nutrients and CO_2 (Toggweiler and Samuels, 1995) that fuel primary productivity. However, the biological uptake of these nutrients is far from complete, with much of the Southern Ocean containing high nutrient concentrations and low phytoplankton biomass. These conditions make the Southern Ocean the largest high-nutrient, low chlorophyll (HNLC) region in the world ocean. The surface waters of the Drake Passage and of the mid- to outer-shelf of the AP are severely iron limited (< 0.1 nmol kg-1; Klunder et al., 2014; Annett et al., 2017) thereby restricting phytoplankton growth. In turn, in the Bransfield Strait and coastal systems of the AP, re-suspension of iron-rich sediments and melting of glaciers result in generally iron replete waters that support high primary production (Ardelan et al., 2010).

2. Material and methods

2.1. The POWELL-2020 campaign

The POWELL-2020 campaign took place onboard the R/V Hespérides from 2 January to 4 February 2020. During the POWELL2020 campaign, 150 stations were sampled during the crossing of the Drake Passage, in the Bransfield Strait, and in the Powell Basin. In these areas, seawater samples were collected from the ship's continuous intake at 5 meters depth. During the southbound transit, surface seawater samples were collected every 3–4 hours to capture key changes across the different ACC fronts. On the return (northbound) transit, sampling was conducted every 2 hours. Within the Bransfield Strait and Powell Basin, sampling intervals were generally every approximately 4 hours, adjusted according to other ongoing research activities.

Three types of filters were used: the 0.45-micron HAWG filter for diatoms, coccolithophores, and dinoflagellates; the 0.45-micron HAWP filter for other organisms; and GFF

filters for pigments, suspended material, and carbon/nitrogen isotopes. Pigments, C/N isotopes, and HAWP filters were stored in aluminium foil and Petri dishes at -80°C, following rapid freezing with liquid nitrogen. The filters for phytoplankton were stored at room temperature in Petri dishes and left to dry for two days.

2.2 Nutrient analysis

During the POWELL-2020 campaign, samples were collected in the Drake Passage and the Bransfield Strait, spanning transects between 65°W and 60°W and from 55°S to 63°S (Fig. 1). Discrete surface water samples were collected at a depth of approximately 5 meters using the underway seawater system. The sampling effort included 140 surface stations distributed approximately every 60 km along the cruise track. Only nutrient data for the 51 stations used for phytoplankton analysis (see section 2.4) are presented here. All samples intended for nutrient analyses were filtered immediately onboard through Whatman polycarbonate membrane filters (0.45 μm pore size, 47 mm diameter) to remove particulate material. The filtered samples were frozen at -20°C in 50ml polyethylene vials for N and P nutrients, while they were stored at room temperature for Si measurements. Nutrient concentrations were analysed at UMR EPOC, University of Bordeaux, and measured using two segmented flow autoanalyzer's from Seal Analytical: the AA3HR macroflow analyser was used for the determination of silicates and phosphates, while the quAAtro microflow analyser was used for the determination of nitrites, nitrates, and ammonium, following the protocol of Bendschneider and Robinson (1952) optimized by Aminot et al. (2009). Silicate determination was based on the formation of a silicomolybdate complex, which is reduced by ascorbic acid to form molybdenum blue. Potential interferences from phosphates were eliminated by adding oxalic acid.

Absorbance for silicates was measured at 820 nm. Phosphate detection was established on the fact that phosphates form a phospho-molybdate complex in the presence of antimony, which is reduced by ascorbic acid to produce an intense blue colour. Absorbance was measured at 880 nm. In comparison, nitrites react under acidic conditions with sulphanilamide and N-naphthyl-ethylenediamine (NED) to form a coloured azo dye. Absorbance was then measured at 540 nm. In parallel, nitrates are quantitatively reduced to nitrites using a cadmium-copper reduction column. The resulting nitrites are then measured using the same colorimetric method as for direct nitrite analysis with an absorbance at 550 nm.

As estimating water density was not feasible for all stations, nutrient concentrations are presented in micromoles per liter (μ M L⁻¹). Conversion from micromoles per liter (μ M L⁻¹) to micromoles per kilogram (μ M kg⁻¹) at selected stations resulted in differences of less than 3% between the two units, implying that the data from this study and that of Freeman et al. (2019) presented in Table 1 in μ M kg⁻¹ are comparable.

2.3 Phytoplankton analysis

Discrete samples were collected from the prefiltered and uncontaminated seawater line taken under the ship at 5 m water depth, in one L Nalgene bottles, and filtered immediately through 0.45-micron pore size, 25 mm diameter HAWG gridded mixed cellulose ester membrane filters. Here we present results from 51 stations representative of the main environments sampled during the POWELL-2020 survey. Filters were placed in polystyrene petri dishes and allowed to dry (24-48 hours). Filters were then cut in half, with one half mounted on a glass slide using immersion oil and covered with a cover slip. These slides were used for quantitative analysis of micro- and nannoplankton abundance and assemblage composition using light microscopy at 1000x magnification for diatoms and a microscope equipped with both linear and

circular polarization at 1000x for coccolithophore identification. The other half of each filter was stored in the petri dish for Back Scattered Electron Imagery analysis using a Hitachi TM4000 Plus SEM. SEM work of selected samples was conducted to clarify identification of smaller specimens.

In regard to the taxonomic identification of diatoms, each diatom cell (i.e. frustule) was identified to the lowest taxonomic level possible using the taxonomic concepts of Hasle and Syvertsen (1997) and Scott and Marchant (2005). Morphological and molecular analyses by Lundholm and Hasle (2008) revealed that Fragilariopsis cylindrus and Fragilariopsis nana are different species but often they share many morphological characteristics that make their differentiation impossible with light microscopy. Therefore, we followed the approach of Cefarelli et al. (2010) lumping the cell counts of these two species under the name F. cylindrus/nana. In regard to the genus Chaetoceros, three groups were distinguished. The vegetative cells of Chaetoceros subgenus Phaeoceros (which includes C. aequatorialis, C. atlanticus, C. criophilus, C. peruvianus, C. dichaeta, C. pendulus, and C. bulbosum) and Hyalochaete were separated owing to their different habitats (oceanic and neritic, respectively). The resting spores of genus Chaetoceros were identified only to group level due to a lack of morphological criteria. In regard to coccolithophore identification, the taxonomic concepts of Young et al. (2003) and Nannotax website (Young et al., 2024) were followed. The lower coccolithophore diversity observed in our study compared to previous work in the study region (e.g. Charalampopoulou et al., 2016) is attributed to methodology applied. Previous studies used Scanning Electron Microscopy that allow for a more precise identification of coccolithophore species as well as identification of different Emiliania huxleyi and Calcidiscus leptoporus morphotypes. In turn, although light microscopy applied in HAWG filters allows a reliable quantification of coccospheres and characterization of most coccolithophore taxa to genus level, it precluded the identification to species and morphotypes level in some cases (e.g. classification of E. huxleyi or C. leptoporus morphotypes). Lastly, it should be acknowledged that the zooplankton community was not analyzed during our survey and therefore their potential influence on phytoplankton standing stocks through grazing could not be assessed.

2.4. Satellite-derived and reanalysis data

246

247

248

249

250

251

252

253

254

255

256

257

258

259

260

261

262

263

264

265

266

267

268

269

270

271

272

273

274

275

276

277

278

279

280

281

282

283

284

285

286

287

288

289

290

291

European Space Agency (ESA) Climate Change Initiative (CCI) and Copernicus Climate Change Service (C3S) SST data spanning from 1982 to 2021 (Merchant et al., 2019; https://doi.org/10.48670/moi-00169; last accessed: May 2025) was used to analyze warm water anomalies. This satellite-derived, reprocessed Level 4 (L4) product provides global, gap-free daily SST at a 0.05° × 0.05° horizontal resolution, allowing for a comprehensive spatiotemporal characterization of MHWs worldwide (e.g. Martínez et al., 2023; Bell et al., 2024; Fernández-Barba et al., 2024). MHWs were then identified based on the methodology outlined by Hobday et al. (2016) and Oliver et al. (2021), with the additional criterion of the long-term mean summer temperature (LMST), as described by Fernández-Barba et al. (2024). Specifically: (i) SSTs must exceed the seasonally varying 95th percentile (relative to 1982-2012), (ii) for a minimum duration of 5 consecutive days, (iii) with gaps of less than 3 days, and (iv) the mean SST must be higher than the LMST. The rationale for including this additional criterion was to exclude winter MHW events, thereby retaining only those that occurred during the austral summer, the season during which the POWELL-2020 campaign took place. As discrete yet prolonged events, MHWs occurred over defined periods during which SST exceeded a specified threshold (the 95th percentile in this work). Therefore, MHW events were spatiotemporal characterized using metrics widely applied in previous studies (see Oliver et al., 2018; Oliver et al., 2021). In our study, MHW duration was calculated as the time interval (in days) between the onset and the

end of each event. Since more than one event may occur within a given year, we also calculated total annual MHW days, defined as the sum of all days in a year during which SST exceeded the MHW threshold. Maximum intensities of MHWs were also calculated as the greatest difference between the absolute temperature and the seasonally varying threshold during each event. Based on this metric, MHW events were categorized according to the number of times the maximum intensity exceeded the difference between the climatological mean and the 95thpercentile threshold (Hobday et al., 2018; Oliver et al., 2021). Thus, events were classified from category 1 to 4 as moderate, strong, severe, and/or extreme, respectively. Additionally, to assess the strength of each event, MHW cumulative intensity was calculated by integrating the event's intensity over its duration. This metric is particularly relevant for evaluating the biogeochemical impacts resulting from MHWs (Oliver et al., 2021; Smith et al., 2023). The general Python code used to detect MHWs is publicly accessible at https://github.com/ecjoliver/marineHeatWaves. The adapted code for the Southern Ocean is also freely available https://github.com/ManuFBarba/Southern-Ocean-MHWs.

To assess the influence of regional ocean dynamics, particularly mesoscale eddies, on the development of the 2020 MHW in the Drake Passage, satellite altimetry-derived variables from the Copernicus Marine Service (CMS) Global Ocean Gridded L4 Sea Surface Heights and Derived Variables product were analyzed. This dataset merges Level 3 along-track altimetric observations from multiple satellite missions into a global gridded product with a spatial resolution of 0.125° × 0.125° (https://doi.org/10.48670/moi-00148; last accessed: May 2025). Specifically, sea level anomaly (SLA) and absolute dynamic topography (ADT) were obtained for the period 1993–2021. These variables provide a first-order approximation of mesoscale circulation patterns modulating the upper-ocean thermal structure. Positive SLA values are typically associated with warmer surface conditions, while negative anomalies generally indicate cooler waters, reflecting the thermal imprint of eddy-driven dynamics (Beech et al., 2022; He et al., 2024). SLA was derived relative to a 20-year mean dynamic topography (MDT) baseline (1993–2012), following the equation:

SLA = SSH - MDT

292

293

294

295

296

297

298

299

300

301

302

303

304

305

306

307

308

309

310

311

312 313

314

315

316

317

318

320

321

322

324

325

328

329

330

Where SSH is the instantaneous sea surface height, and MDT represents the long-term mean difference between sea level and the geoid (equipotential surface). Then, ADT corresponds to the absolute sea surface height referenced to the geoid, given by:

$$ADT = SLA + MDT$$

ADT is directly related to the geostrophic surface velocity field. The zonal (u_g) and meridional (v_g) components of geostrophic velocity were computed as:

Where g is the gravitational acceleration, f is the Coriolis parameter ($f=2\Omega\sin\phi$; $\phi=$ latitude). Then, to further characterize mesoscale activity, Eddy Kinetic Energy (EKE) was computed from geostrophic velocity anomalies.

331
$$EKE = \frac{1}{2} (u_g^{\prime 2} + v_g^{\prime 2})$$

Where $u_g'=u_g-\langle u_g\rangle$ and $v_g'=v_g-\langle v_g\rangle$ represent the deviations from the long-term mean geostrophic velocities ($\langle u_g\rangle$ and $\langle v_g\rangle$, respectively). Moreover, to quantify kinetic energy redistribution throughout the water column, Vertically-Integrated Kinetic Energy (VIKE) was computed as:

336
$$VIKE = \int_{z_1}^{z_2} \frac{1}{2} \rho(u^2 + v^2 + w^2) dz$$

Where ρ is the seawater density profile, obtained from the CMS Global Ocean Physics Reanalysis (https://doi.org/10.48670/moi-00021; last accessed: May 2025) at 0.083° x 0.083° horizontal resolution, and u, v, and w are the three-dimensional velocity components. VIKE is a critical diagnostic to quantify the contribution of mesoscale eddies to the vertical energy structure of the ocean and their potential role in modulating SST and triggering MHWs (Bian et al., 2023).

To investigate the atmospheric drivers, radiative fluxes, and surface energy inputs contributing to the onset of the 2020 MHW in the Drake Passage, key variables from the European Centre for Medium-Range Weather Forecasts (ECMWF) ERA5 reanalysis product, provided by the C3S (Hersbach et al., 2023; https://doi.org/10.24381/cds.adbb2d47; last accessed: May 2025) were analyzed. This global reanalysis combines model outputs with observational data to generate a product at 0.25° x 0.25° horizontal resolution, which has been extensively validated in the Southern Ocean and has outperformed other reanalyses (Gossart et al., 2019; Tetzner et al., 2019; Zhu et al., 2021). Specifically, anomalies of variables directly linked to heat transfer (2m-Air temperature and 10m-Wind Speed), radiative forcing (Surface net shortwave radiation flux, Surface net long-wave radiation flux, Surface downward short-wave radiation flux, and Surface downward long-wave radiation flux), and surface sea-air dynamics (Mean sea level pressure, Surface latent heat flux, Surface sensible heat flux, Turbulent surface stress, and Normalized energy flux into ocean) were calculated relative to a 31-year reference period (1982-2012).

To support our *in-situ* data, net primary production (NPP) data was obtained from the Copernicus Global ocean low and mid trophic levels biomass content hindcast (https://doi.org/10.48670/moi-00020; last accessed: May 2025). This product combines interpolated L4, multi-satellite data with reanalysis data to provide daily fields at a spatial resolution of approximately 8 km. To enable comparison with *in-situ* observations and to reinforce the interpretation of local variability, monthly modeled surface dissolved iron concentration from the Global Ocean Biogeochemistry Hindcast dataset (https://doi.org/10.48670/moi-00019; last accessed: May 2025), at 0.25°×0.25° horizontal resolution was also incorporated.

2.5 Statistical analyses

Canonical Correspondence Analysis (CCA; ter Braak and Verdonschot, 1995) was used to explore the relationship between the relative abundance of diatom species and measured environmental parameters. This analysis is a constrained ordination technique that combines simultaneously the ordination of diatom species, stations and environmental parameters. Diatom species with more than 1% relative abundance in at least one sample were selected for the analysis; while the following key environmental parameters were selected for this analysis: latitude, SST, SSTA, salinity, fluorescence and the macronutrients silicate, phosphate and nitrate. Stations with missing environmental data were removed from the analysis, resulting in a final

dataset that contained 39 stations. The analysis was conducted using R v4.5.0, R Core Team (2025).

To evaluate the possible influence of the MHW affecting the Drake Passage in summer 2020, sampling stations of the Drake Passage were organized into four groups: stations north of the Polar Front sampled before (i) and during the onset of the MHW (ii) and stations south the Polar Front before (iii) and during the onset MHW (iv). Due to the absence of normality of the numerical variables, the non-parametric Wilcoxon test was used to determine differences in key physical and chemical parameters, diatom and coccolithophore cell concentrations and in the relative abundance of key diatom species before and during the marine heat wave in the Drake Passage.

3. Results

3.1 Nutrient distributions

Nutrient distributions in the surface layer across the Drake Passage and Bransfield Strait during January and early February 2020 are illustrated in Figure 2b and summarized in Table 1. During the southbound transit to the Shetland archipelago in early January 2020, nitrate concentration in the subantarctic and polar frontal zone waters ranged between 7.6 and 14.3 and between 9.0 and 17.2 μ mol L⁻¹, respectively, while phosphate concentrations ranged between 0.7 and 1.3 and between 1.3 to 1.4 μ mol L⁻¹, respectively. Silicate concentration was low in the subantarctic zone and in the PFZ (with values ranging between 2.2 to 2.8 μ mol L⁻¹, and between 1.3 to 2.1 μ mol L⁻¹, respectively). South of the Polar Front, nitrate and phosphate levels showed a slight increase (from 13.0 to 17.4 and from 1.4 to 1.7 μ mol L⁻¹, respectively), whilst roughly a ten-fold rise in silicate concentrations (11.7-21.6 μ mol L⁻¹) was observed. This sharp silicate gradient at the PF is also known as the Silicate Front and represents a critical boundary for nutrient distributions in the Southern Ocean (Freeman et al., 2019; Table 1). South of the SB and in the Bransfield Strait, nitrate and phosphate levels exhibit concentrations similar to those documented in the AZ waters (Fig. 2b). In turn, silicate concentrations exhibited the highest levels of the meridional gradient, with values up to 77.0 μ mol L⁻¹ (Fig. 2b).

During the northbound transit in late-January early-February, the main biogeochemical Southern Ocean zones remained clearly evidenced in the nutrient distributions. However, some important differences compared with the southbound transit were noticed. Nitrate levels in the northern AAZ and north of the PF decreased about one order of magnitude (down to $0.8~\mu mol~L^{-1}$) compared to those registered in the southbound transit. Likewise, phosphate concentrations also decreased substantially north of the PF (down to $0.6~\mu mol~L^{-1}$). In contrast, the meridional distribution of silicate remained similar to that documented in the southbound transit (Fig. 2b).

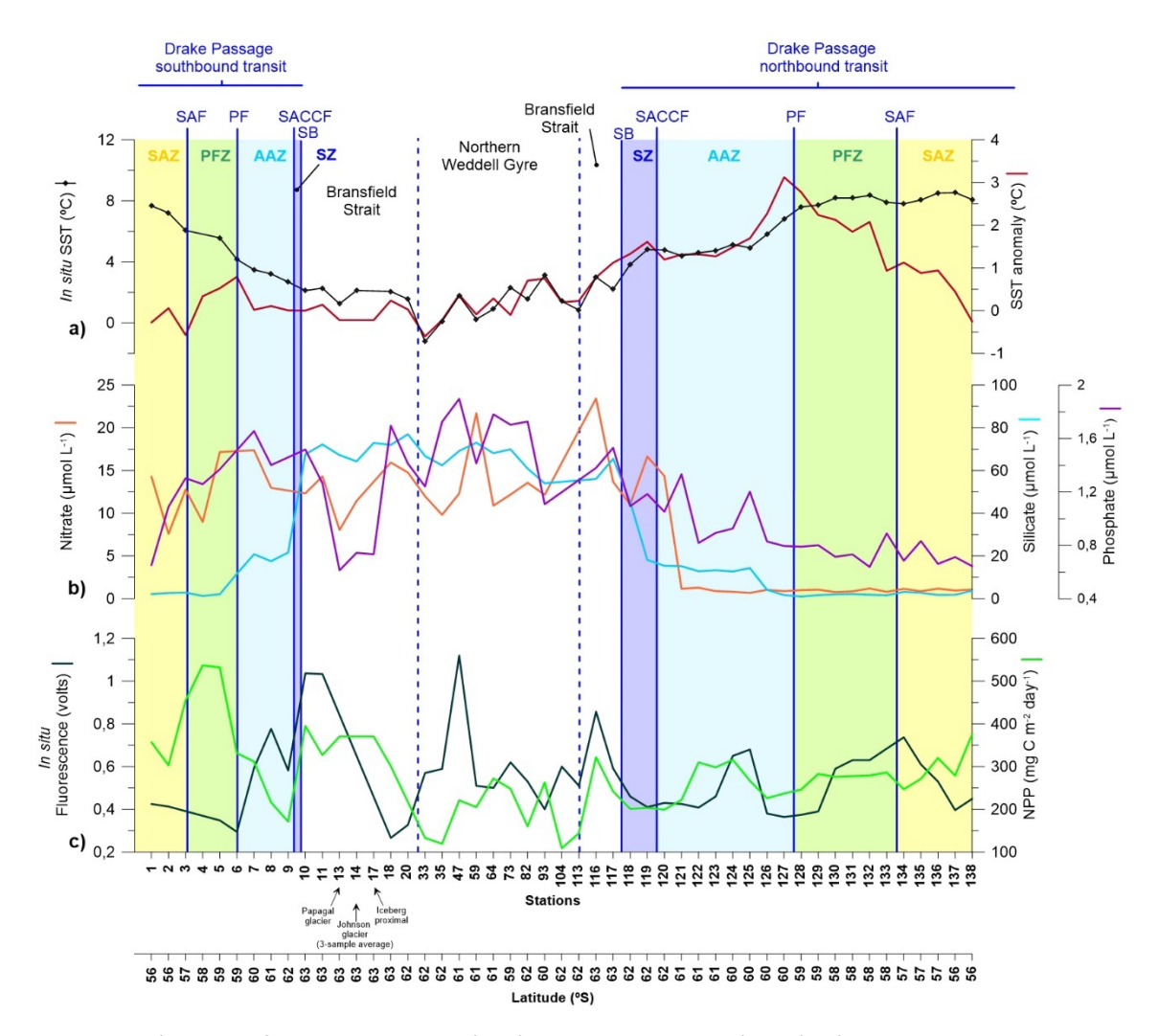


Figure 2. a) Sea Surface Temperature (SST) and SST anomaly (SSTA). b) nutrient concentrations (nitrate, silicate and phosphate). c) Fluorescence (*in situ*) and net primary production (NNP).

Table 1. Physical and chemical parameters of the Drake Passage. Interannual average values represent the median and first and third quartiles (between brackets) for silicate, nitrate, phosphate, temperature and salinity between 2004 and 2017 from Freeman et al. (2019) and for Mixed Layer Depth (MLD) between 2004 and 2011 from Stephenson et al. (2012). Variability range of each parameter during the outbound (early January 2020) and northbound transits (Late-January early-February 2020) of the Powell-2020 campaign. *Freeman et al. (2019) and Stephenson et al. (2012) do not cover the Bransfield Strait but data from this region is presented for the POWELL-2020 campaign.

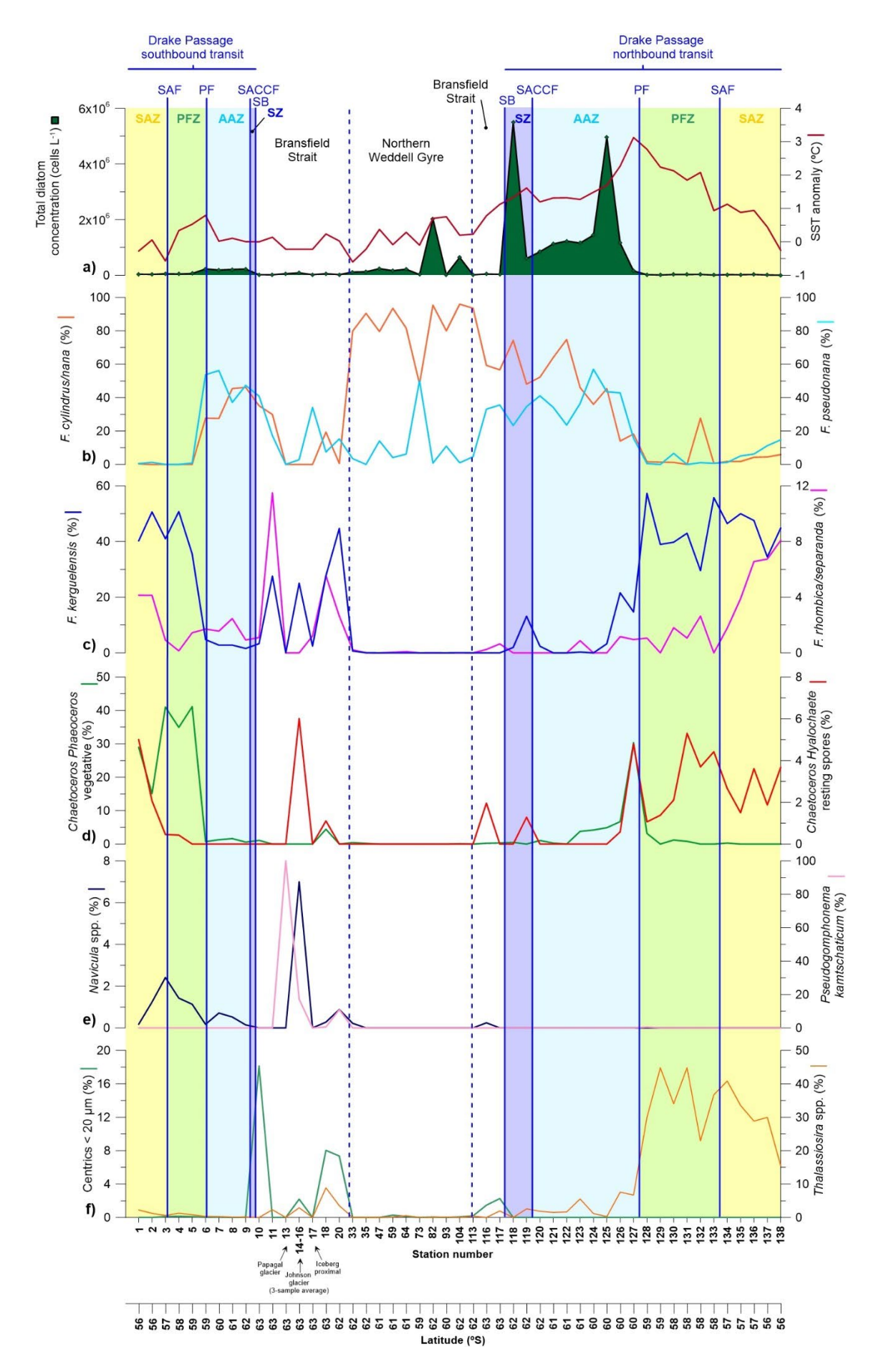
Zonal					Temperature			
system	Time interval	Silicate	Nitrate	Phosphate	(°C)	Salinity (psu)	MLD (m)	Stations
SAZ	Interannual average	4.6 (3.0–6.5) μmol/kg	20.6 (19.0-21.4) µmol/kg	1.5 (1.4–1.5) µmol/kg	5.6 (5.0-6.0)	34.1 (34.0-34.1)	141.4 (87.1-225.8)	-
	Early January 2020	2.17-2.82 μmol/L	7.6-14.3 µmol/L	0.65-1.30 µmol/L	6.06-7.67	33-33.6	-	1-3
	Late-January early- February 2020	1.77-3.76 μmol/L	0.87-1.17 μmol/L	0.65-0.83 μmol/L	7.8-8.54	33.10-33.60	-	134-138
PFZ	Interannual average	6.7 (4.1-9.8) µmol/kg	22.8 (21.5-24.2) µmol/kg	1.6 (1.5–1.7) μmol/kg	4.5 (3.8-5.3)	34 (34.0-34.1)	82.7 (44.6-144.4)	-
	Early January 2020	1.28-2.08 μmol/L	8.98-17.16 µmol/L	1.26-1.37 µmol/L	5.57	33.5	-	4-5
	Late-January early- February 2020	1.6-2.2 μmol/L	0.77-1.2 μmol/L	0.64-0.89 μmol/L	7.6-8.35	33.4-34.8	-	128-133
AAZ	Interannual average	21.6 (16.0-29.6) µmol/kg	25.7 (24.7-26.8) µmol/kg	1.7 (1.7-1.8) µmol/kg	0.7 (-0.7-1.9)	33.8 (33.7-33.9)	70.7 (48.3-99.4)	-
	Early January 2020	11.69-21.6 µmol/L	12.97-17.37 μmol/L	1.4−1.66 µmol/L	2.68-4.16	33-33.5	-	6-9
	Late-January early- February 2020	1.7–15.4 μmol/L	0.68-14.36 μmol/L	0.8-1.33 μmol/L	4.40-6.8	33-33.8	-	120-127
SZ - Bransfield Strait*	Interannual average	40.5 (27.4-52.3) µmol/kg	26.3 (23.9-27.8) µmol/kg	1.8 (1.7-2.0) µmol/kg	-0.5 (-1.3-1.0)	33.9 (33.8-34.0)	75 (58.3-96.4)	-
	Early January 2020	64.28-76.96 µmol/L	8.04-15.93 μmol/L	0.61-1.70 μmol/L	1.25-2.28	31.8-33.9	-	10-20
	Late-January early- February 2020	18.14–65.49 µmol/L	11.02-23.43 µmol/L	1.09-1.53 µmol/L	2.2-4.8	33.2-33.5	-	116-119

3.2 Phytoplankton abundance variability

In-situ fluorescence measurements at 5 m depth from the ship (Fig. 2c) indicate maximum algal biomass accumulation in the western Bransfield Strait (in both the southbound and northbound transits) and in the Weddell Sea. In terms of temporal variability in the Drake Passage (i.e. before and during the onset of the MHW), average fluorescence suggests slightly higher algal biomass accumulation in the southbound and northbound transits (0.61 and 0.53 volts in the southbound and northbound transits, respectively) and 0.55 volts in the Bransfield and Northern Weddell Sea. Likewise, modelled NPP suggests higher values in the southbound transit (358 mg C m⁻² day⁻¹) than in the northbound transit (269 mg C m⁻² day⁻¹; Fig. 2c).

In terms of diatom distributions, total diatom abundance ranged between 0.003 and 5.5 x 10^6 cells L⁻¹ and exhibited a clear increase south of the PF (Fig. 3a). In terms of temporal distribution, diatom abundance within the same zonal systems was generally lower during early January than in late-January and early-February. While there is no universally fixed threshold for what constitutes a phytoplankton bloom, a frequent definition is a proliferation event with cell concentrations reaching or exceeding one million cells per Liter (e.g. Johnsen et al., 1999). Based on this definition, diatom bloom concentrations during the POWELL-2020 campaign were reached during the second half of the expedition in one station in the Bransfield Strait (station 82; Fig. 3a) and, almost consistently, during the northbound transit in the Southern Zone and Antarctic Zone (stations 118-126; Fig. 3a), with cell numbers reaching values up to ca. 5.5 x 10^6 and 5×10^6 cells L⁻¹, respectively.

Coccolithophore abundance was low compared to diatoms, with cell concentrations ranging between 0 and 8 x 10^4 coccospheres L^{-1} (Fig. 4a). Our results reveal a nearly opposite latitudinal distribution than that of the diatoms, with maximum concentrations in the SAZ and PFZ. Coccolithophore abundance was negligible in the Bransfield Strait and northern Weddell Sea, with no coccospheres documented during our counts although a few coccospheres where identified (but not quantified) during SEM analyses. In regard to temporal variability, average coccolithophore abundance in the SAZ and PFZ was two-fold during the southbound transit in early January (4.2 x 10^4 coccospheres L^{-1}) than during the northbound transit in late January-early February (ca. 1.6×10^4 coccospheres L^{-1}). Coccolithophore assemblages were composed of two species: *E. huxleyi* and *C. leptoporus*.



464

465

466

467

468

469

470

471

472

473

474

475

476

477

478

479

456

457

458

459

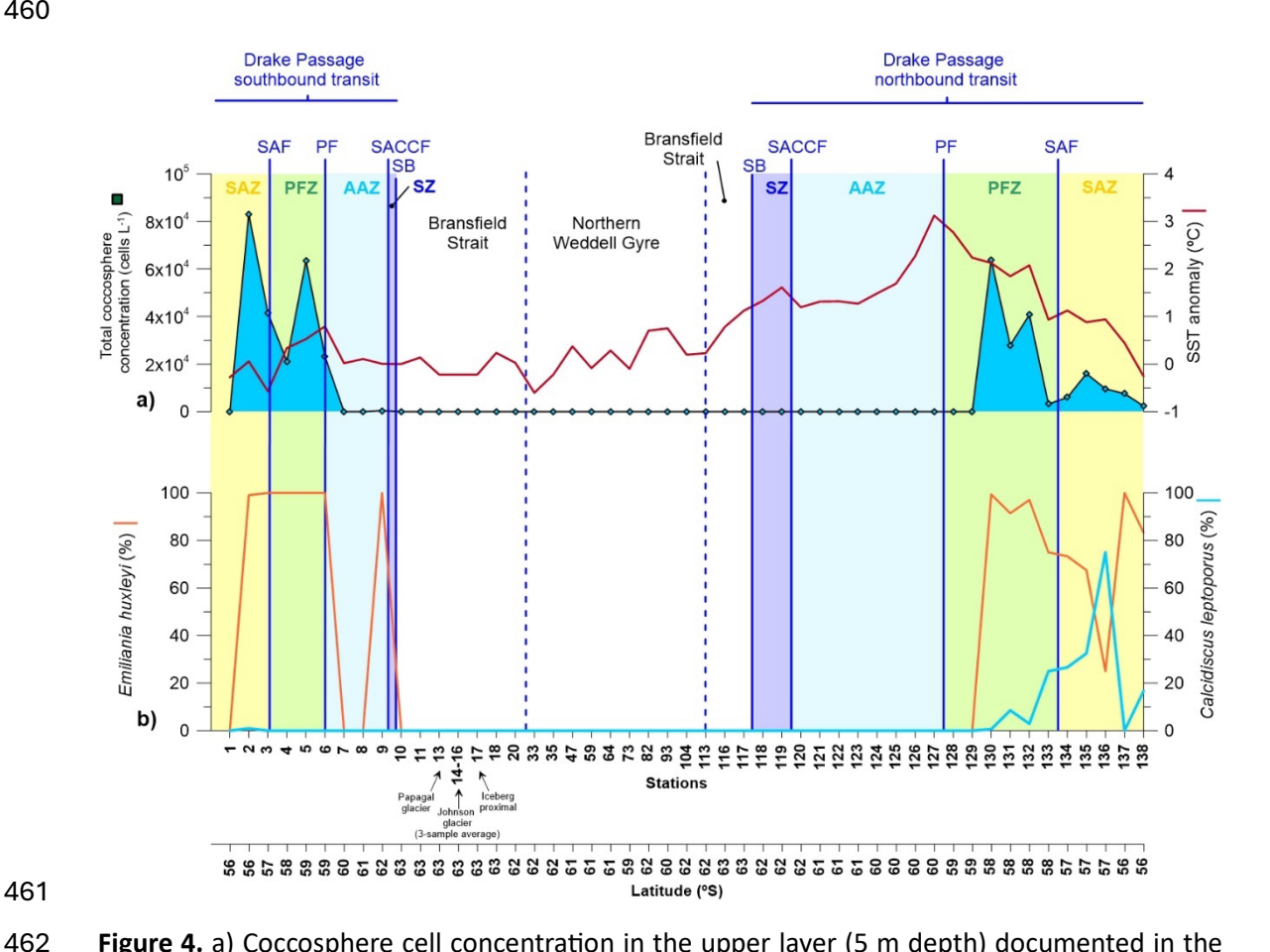


Figure 4. a) Coccosphere cell concentration in the upper layer (5 m depth) documented in the Drake Passage, Bransfield Strait and Northern Weddell Sea Gyre documented in representative stations of main environments during the POWELL-2020 campaign. b) Relative abundance of Emiliania huxleyi and Calcidiscus leptoporus.

3.3 Distribution of phytoplankton species

Fragilariopsis kerguelensis dominated the diatom assemblages in the SAZ and PFZ (i.e. north of the PF) in both the southbound (average of 44%) and northbound transits (average of 44%). South of the polar front, F. kerquelensis exhibited relatively high concentrations in some stations of the western Bransfield Strait during early summer (up to 45% in station 20; Fig. 3c). Fragilariopsis cylindrus/nana and Fragilariopsis pseudonana displayed a nearly opposite pattern to that of F. kerquelensis, dominating the diatom assemblages in most of the stations south the PF. Fragilariopsis cylindrus/nana contributed an average of 51% to the diatom assemblage in all the stations south of the PF, reaching maximum abundances in the northern Weddell Sea stations where its contribution accounted for up 96% of the total diatom assemblage (station 104; Fig. 3b). F. pseudonana contributed on average 24% of the diatom assemblage south of the PF, with peak contributions in the Antarctic Zone. In terms of temporal variability, some differences between the southbound and northbound transits were noticed. While F. cylindrus/nana represented an average of 35% of the diatom assemblage from the PF

southwards in the Drake Passage in early January 2020 (i.e. the southbound transit), the relative abundance of this taxon increased to 49% in the same zonal systems during the onset of the MHW (i.e. northbound transit; Fig. 3b). In turn, *F. pseudonana* exhibited a slight decrease in its relative contribution reaching an average relative contribution in the southern Drake Passage between the southbound (42%) and the northbound transit (35%).

480

481

482

483

484

485

486

487

488

489

490

491

492

493

494

495

496

497

498

499

500

501

502

503

504

505

506 507

508

509

510

511

512

513

514

515

516

517

518

519

520

521

522

523

524

525

526

Chaetoceros subgenus Phaeoceros was a major component of the diatom community in the SAZ and PFZ during the southbound transit (average of 32% of the total diatom assemblage; Fig. 3d). In turn, this taxon only exhibited an average contribution of 3% during the northbound transit with elevated numbers recorded only at one station (station 127 with a contribution of 30%). The vegetative cells of Chaetoceros subgenus Hyalochaete were only documented in abundances over 1% in the first two stations of the SAZ (stations 1 and 2, with 6 and 2%, respectively; data not shown). Chaetoceros resting spores showed a contrasting distribution in the Drake Passage between the southbound and northbound transits. During the southbound transit, they were only present in the SAZ (up to 5%) and northern PFZ (Fig. 3d), while during the northbound transit they were consistently documented between the northern AAZ and SAZ (ranging between 1 and 5%). Chaetoceros resting spores were also present in some stations in the Bransfield Strait (up to 6% in Livingston Island). Notably, the diatom assemblages collected near Papagal and Johnson glaciers in the coastal waters of Livingston Island (stations 13 and 14) were remarkably different from the rest of the stations and rich in fine sediments. These samples exhibited high abundances of Pseudogomphonema kamtschaticum (average of 38%) and secondary contributions of Navicula spp. (5%). The small centric group (that encompasses all small centric diatoms under 20 µm that were not identified to a lower taxonomic level) exhibit peak values south of the SB and in the Bransfield Strait in early January, reaching values up to 18% in station 10. Interestingly, SEM imagery revealed that some of the small centrics were Minidiscus chilensis, although it was not possible to quantify its contribution due to the limitations of light microscopy. Lastly, *Thalassiosira* spp. was a major contributor of the diatom assemblages in the PFZ and SAZ during the southbound transit accounting for up to 45% of the diatom assemblage in the SAZ (Fig. 3f).

The first two axes of the CCA explain 72.9 % of the variability in species distribution based on the environmental gradients; with CCA1 and CCA2 axes accounting for 59.3% and 13.6% of the total inertia (Fig. 5). Axis CCA1 is mainly correlated with SST (negatively), latitude (negatively), silicate (positively), phosphate (positively) and nitrate (positively), while CCA2 was mainly correlated with nitrate (positively), and to a lower extent with SSTA (negatively), Fluorescence (negatively) and Salinity (negatively). The sampling stations are clearly grouped in the CCA ordination triplot; with all the stations north of the Polar Front (i.e. stations in the SAZ and PFZ) located on the left side of the triplot and the majority of the samples south of the Polar Front on the right side. Diatom species resting on the negative side of CCA1 are positively correlated with SST and low latitudes (please note that latitude is expressed in negative values in the Southern Hemisphere) and negatively correlated with the three nutrients analysed. The most relevant species on the negative side of CCA1 are Nitzschia bicapitata, Nitzschia sicula, Chaetoceros Hyalochaete vegetative and resting spores, Thalassiosira gravida, Thalassiosira lentiginosa, Centrics > 20µm; Thalassiosira spp., Fragilariopsis kerguelensis, Fragilariopsis sublinearis, Chaetoceros Phaeoceros vegetative, Fragilariopsis rhombica/separanda, Pseudo-nitzschia turgiduloides and Rhizosolenia spp.. In turn, Fragilariopsis vanheurckii, small Fragilariopsis spp., Fragilariopsis curta, Fragilariopsis cylindrus/nana, Corethron sp., Centrics < 20 μm, Fragilariopsis pseudonana, and Fragilariopsis spp. are placed on the positive side of CCA1 reflecting their affinity for greater latitudes, low temperatures, high macronutrient concentrations and to a

lesser degree, enhanced fluorescence. The diatom species *P. kamtschaticum* is placed in the negative side of CCA2 thereby suggesting affinities for higher salinities and lower SSTA and fluorescence. However, it should be noted that peak concentrations of *P. kamtschaticum* were recorded in stations with low salinity owing to meltwater influence (stations 13 to 17), but owing to the lack of measurements of some environmental variables, these stations were excluded from the CCA (see section 4.1 for more details).

527

528

529

530

531

532

533

534

535

536

537

538

539

540

541

542

543

544 545

546

547

548

549

550

551

552

In terms of coccolithophore assemblage composition, *Emiliania huxleyi* largely dominated the coccolithophore assemblages during our survey with an average relative abundance of ca. 87%. In regard to temporal variability of coccolithophores, a contrasting distribution of *C. leptoporus* could be observed between the southbound and northbound transits. *C. leptoporus* contribution was negligible during the southbound transit but increased substantially during the northbound transit, reaching values up to 75% of the coccolithophore assemblage in the SAZ (station 136; Fig. 4).

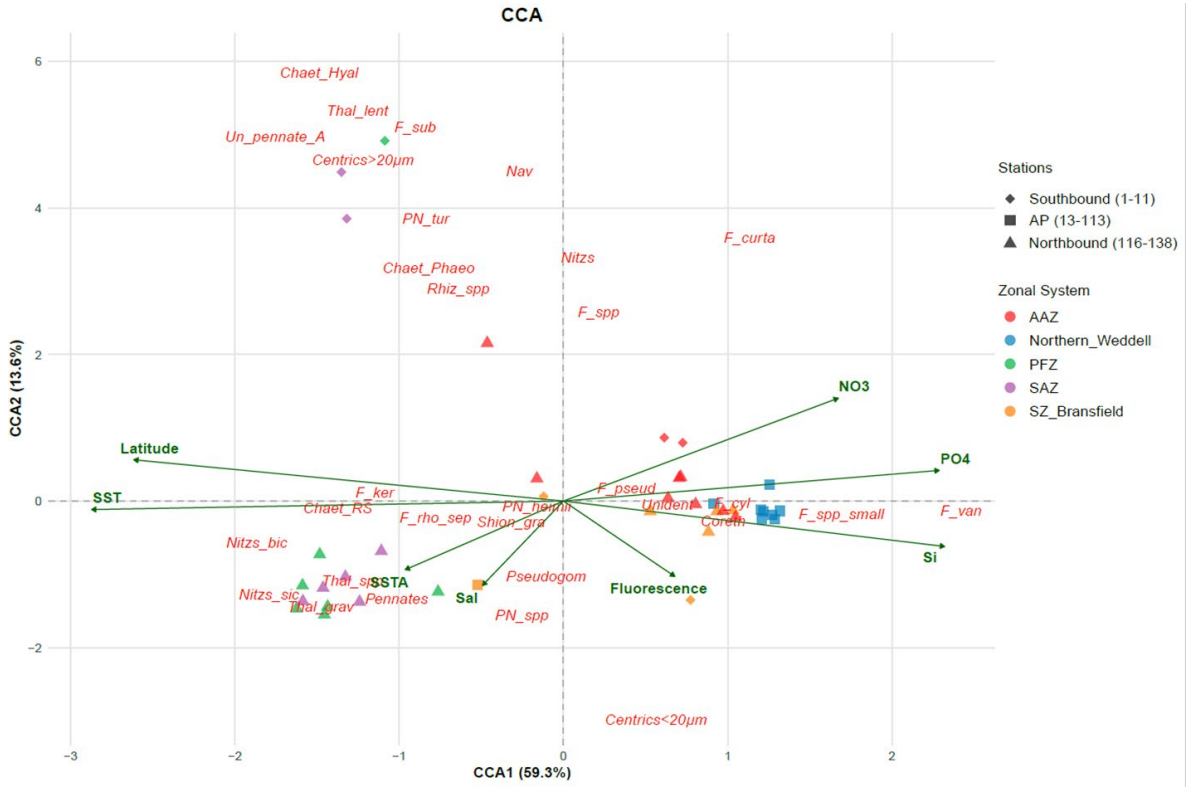


Figure 5. Canonical Correspondence Analysis (CCA) ordination triplot representing key environmental parameters (green arrows); relative abundance of diatom species (red) and sampling stations (dots). Chaet Hyal: Chaetoceros Hyalochaete vegetative cells; Chaet RS: Chaetoceros resting spores; Chaet Phaeo: Chaetoceros Phaeoceros vegetative; Centrics<20µm: Unidentified centrics < 20μm; Centrics>20μm: Unidentified centrics > 20μm; Coreth: Corethron sp.; F curta: Fragilariopsis curta; F cyl: Fragilariopsis cylindrus/nana; F ker: Fragilariopsis kerquelensis; F pseud: **Fragilariopsis** pseudonana; F rho/sep: **Fragilariopsis** rhombica/separanda; F_spp.: Fragilariopsis spp.; F_spp_small: small Fragilariopsis spp.; F_sub: Fragilariopsis sublinearis; F van: Fragilariopsis vanheurckii; Nav: Navicula spp.; Nitzs: Nitzschia spp.; Nitzs bic: Nitzschia bicapitata; Nitzs sic: Nitzschia sicula; Pennates: Unidentified pennates; Pleuro: Pleurosigma spp.; Pn_tur: Pseudo-nitzschia turgiduloides; Pn_spp: Pseudo-nitzschia spp.; Pseudogom: Pseudogomphonema kamtschaticum; Pn heimii: Pseudo-nitzschia heimii; Rhiz_spp: Rhizosolenia spp.; Shion_gra: Shionodiscus gracilis; Thal_grav: Thalassiosira gravida;

Thal_lent: Thalassiosira lentiginosa; Thal_spp: Thalassiosira spp.; Un_pennate_A: Unidentified pennate form A; Unident: Unidentified diatom.

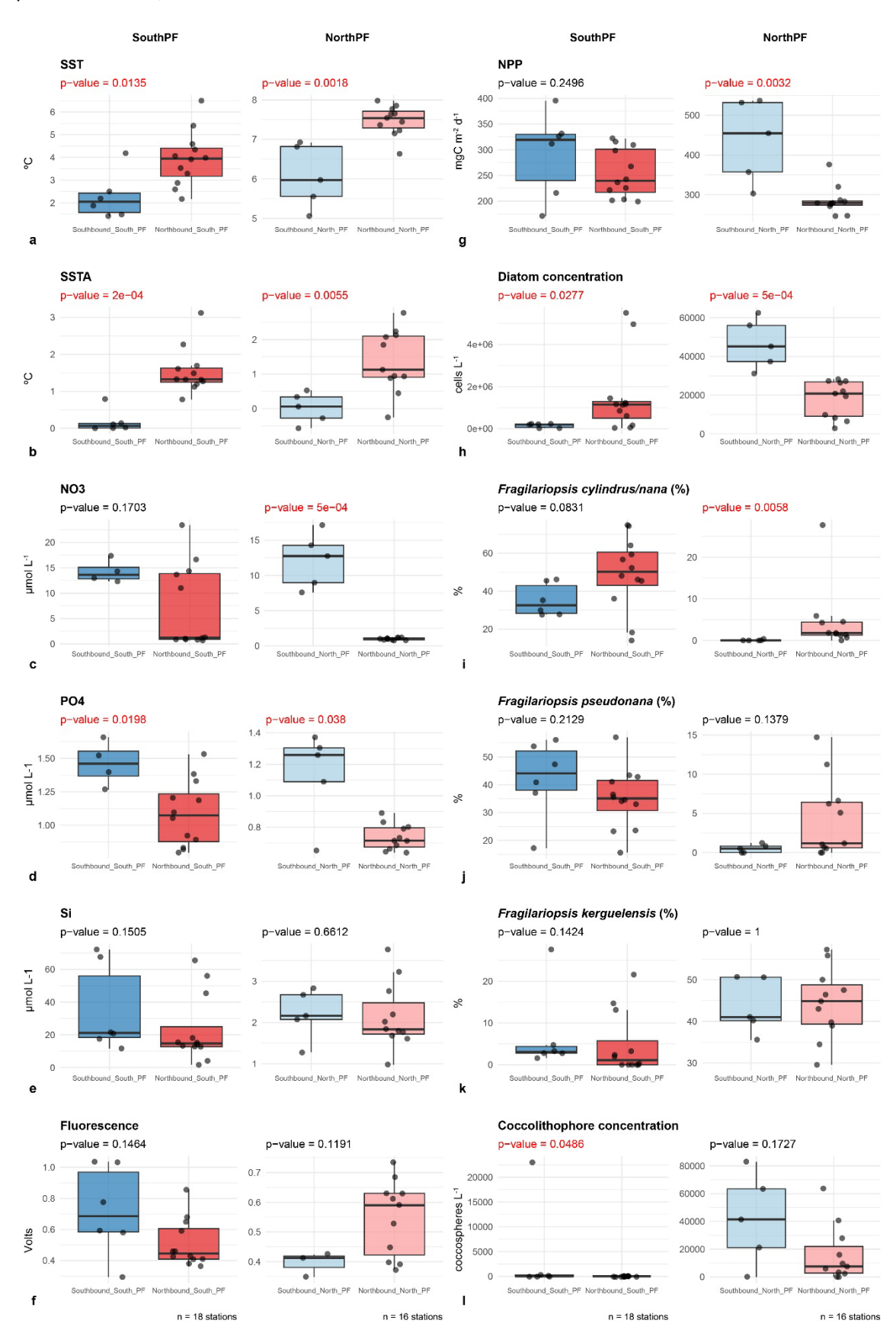


Figure 6. Box plots showing the distribution of key environmental and biological parameters in the northern and southern Drake Passage before (southbound transit) and during the onset of the marine heat wave (northbound transit). The box plots show the lower and upper quartiles, median, minimum, and maximum values, and outliers. p-values in red indicate significant differences between the distributions of the two samples (p < 0.05).

3.4 Characterization of the marine water anomaly

556

557

558

559

560

561

562

563

564

565

566

567 568

569

570

571

572

573

574

575

576

577

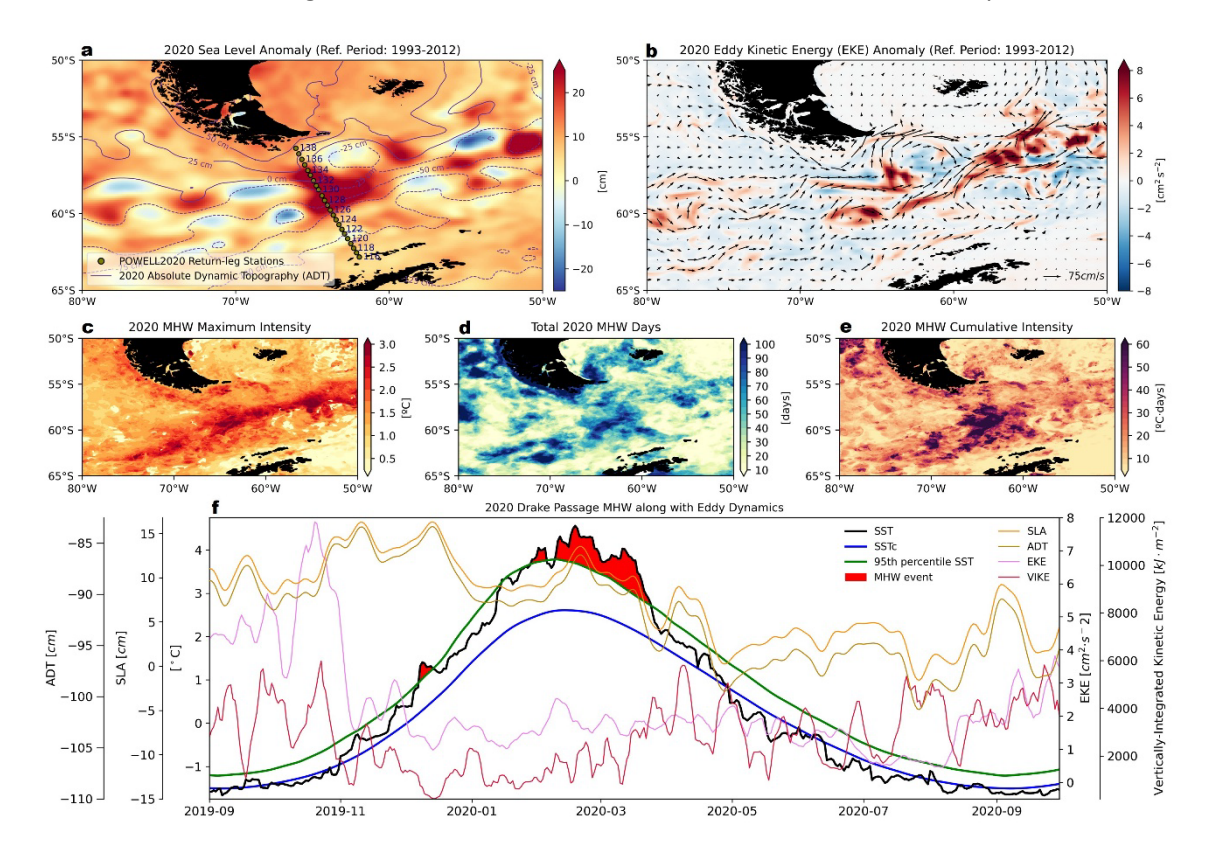
578

579

580

581

In late austral summer of 2020, significant MHWs developed in the Drake Passage (Fig. 7). The SLA field, referenced against the 1993-2012 climatology, revealed positive values along the path of the POWELL-2020 northbound transect (January 31-February 2), exceeding +20 cm (Fig. 7a). Elevated ADT coincided with this SLA signal. EKE anomalies and the configuration of geostrophic surface currents during this period displayed intensified mesoscale activity in the region (Fig. 7b). SST anomalies (SSTA) reached +3 °C above climatological thresholds (Fig. 7c), with MHW intensity falling in the moderate to severe range as defined by Hobday et al. (2018). The event persisted for over 90 days in parts of the Drake Passage (Fig. 7d), with cumulative intensities averaging more than 60 °C days (Fig. 7e). Temporal averages along the POWELL-2020 return transect indicated that SLA and ADT anomalies peaked during the strongest MHW periods (Fig. 7f). EKE values were elevated compared to typical summertime conditions (Fig. 7f). In contrast, VIKE remained relatively low during the MHW peak and increased only after its decline (Fig. 7f). To assess atmospheric variability during the events, near-surface (2-meter) air temperature (N-SAT) anomalies, 10-meter wind speeds, and surface heat fluxes were examined (Supplementary Fig. 1). January 31–February 2, 2020, showed slightly elevated air temperatures (Supplementary Fig. 1a), reduced wind speeds (Supplementary Fig. 1b), and transient increases in shortwave, longwave, latent, and sensible fluxes relative to the 1982-2012 baseline (Supplementary Fig. 1c-h). However, the net surface heat exchange during the onset of the MHWs was predominantly negative ((Supplementary Figs. 1i, 2). Net longwave and latent heat fluxes were also negative, while sensible heat flux showed moderate positive values



(Supplementary Fig. 1i). Wind-induced turbulent stress remained relatively stable during the MHW peaks, increasing only after the event subsided (Supplementary Fig. 1i).

Figure 7. Characterization of the marine thermal anomaly during the austral summer of 2020 in the Drake Passage. (a) Sea level anomalies (SLA; shading) and absolute dynamic topography (ADT; purple contours), averaged over January 31–February 2, coinciding with the return transect of the POWELL-2020 campaign. (b) Eddy kinetic energy (EKE; shading) anomalies and surface geostrophic currents (black arrows) from CMS multi-satellite observations. (c–e) Marine heatwave (MHW) properties during the austral summer of 2020, based on ESA CCI C3S L4 sea surface temperature (SST) using the 95th percentile criterion: (c) maximum intensity, (d) total days, and (e) cumulative intensity. (f) Temporal evolution of SLA (orange), ADT (olive), EKE (pink), and Vertically-Integrated Kinetic Energy (VIKE, dark red), together with MHW events (red shading), as indicated by ESA CCI C3S L4 daily SST (black), climatological SST (SSTc, blue), and MHW criterion (95th percentile SST, green), during 2019–2020. Time series represent spatial averages over the return-leg stations of the POWELL-2020 campaign (green dots in (a)). A 7-day running mean filter is applied to EKE and VIKE. The reference period for the SLA and EKE anomalies is 1993–2012 (a, b, and f), while that for MHWs is 1982–2012 (c–f).

3.5 Impact of the marine heat wave on the environmental and biological parameters in the Drake Passage

Boxplots of the most relevant environmental and biological variables in the two divisions of the Drake Passage before and during the MHW are shown in Figure 6. Wilcoxon's rank-sum tests showed that both SSTs and SSTAs were significantly greater in the Drake Passage (both in northern and southern regions) at the onset of the MHW (Fig. 6a and b). In terms of nutrient distributions, silicate concentrations were fairly similar before and after the MHW in the whole Drake Passage (Fig. 6e). In turn, nitrate concentrations were significantly lower north of the Polar Front during the MHW, while phosphate levels were significantly lower in both north and south the Polar Front during the MHW (Fig. 6c and 6d). In situ fluorescence measurements suggest no significant differences in algal biomass accumulation (Fig. 6f), while NPP was significantly lower in the northern Drake Passage during the MHW (Fig. 6g). In turn, diatom cell concentrations showed contrasting results, exhibiting statistically higher diatom cell numbers south of the Polar Front during the onset of the MHW but lower for the northern Drake Passage (Fig. 6h). In terms of the relative contribution of key diatom taxa, F. cylindrus/nana increased its abundance throughout the Drake Passage during the MHW (Fig 6i). It should be noted that although the difference for the change in the relative abundance of this species was not significant for the region south of the PF, when the two northernmost stations of the AAZ (i.e. 126 and 127) are removed from the analysis, the difference becomes significant (Wilcoxon test p-value = 0.0047; box plot not shown). These results indicate that F. cylindrus/nana increased its relative contribution in the southern Drake Passage during the MHW. Likewise, while F. kerguelensis showed lower relative contribution south of the PF during the MHW (Fig. 6k), the decrease was only significant when the two northernmost stations of the AAZ are not considered (Wilcoxon test p-value = 0.0318; box plot not shown). Lastly, F. pseudonana showed not statistically differences throughout the Drake Passage (Fig. 6j). In terms of coccolithophore distributions, coccosphere concentrations were significantly lower in the southern Drake Passage during the onset of the MHW and lower but not significantly different in the northern Drake Passage (Fig. 6I).

4. DISCUSION

4.1 Environmental variability and phytoplankton species distribution in the Drake Passage and Antarctic Peninsula in summer 2020

The meridional nutrient distributions documented during the POWELL-2020 campaign reflected the changes in water masses depicted by the Southern Ocean fronts. The sharp silicate gradient identified at the Polar Front in both the northbound and southbound transits (Fig. 2b), also known as the Silicate Front, represents the transition between silicate-poor waters to the north and silicate-rich waters to the south (e.g. Trull et al., 2018; Freeman et al., 2019). The poleward increase in nitrate and phosphate concentrations across the Drake Passage in both transits is also consistent with that documented in previous reports (Freeman et al., 2019). However, it is important to note that concentrations for nitrate and phosphate during the POWELL-2020 expedition were lower than average summer values for all the circumpolar systems (Table 1). Nutrient meridional gradients across the Drake Passage were coupled with a decrease of SST (Fig. 2) and close to monotonic changes of other environmental parameters (e.g. pH; Charalampopoulou et al., 2016; Trull et al., 2018).

Overall, the abundance and distribution of the phytoplankton assemblages across the Drake Passage and Bransfield Strait reflected changes in the physical and chemical properties of the water masses delineated by the fronts (Figs. 3, 4 and 5). The increase in diatom abundance south of the PF (Fig. 3) is directly related to the increase in silicate concentrations in the water column that fuel diatom productivity (Landry et al., 2002; Wright et al., 2010; Assmy et al., 2013; Trull et al., 2018). The dominance of F. kerguelensis in the Subantarctic Zone and Polar Frontal Zones (i.e., north of the PF; Fig. 3c and 5) agrees well with previous work in the southwestern Atlantic Ocean where peak relative abundance of this species were documented in the Drake Passage (Cefarelli et al., 2010). However, the meridional distribution in our study is somewhat different from that documented in the southcentral Atlantic, where Froneman et al. (1995) observed maximum contributions of F. kerguelensis south of the Polar Front (i.e. an opposite trend to that observed here; Fig. 3c). The reason for this discrepancy is most likely due to the proliferation of small *Fragilariopsis* species in the southern Drake Passage. Interestingly, F. kerguelensis dominated in areas characterized by low silicate (< 4 μmol L-1) and low iron levels (Supplementary Figure 3) during both the southbound and northbound transits. This finding is surprising because the growth rate of large and heavily silicified diatoms such as F. kerguelensis is limited at silicate concentrations below 5 μ M and substantially curtailed below 2.5 μ M (Frank et al., 2000).

The distribution of *F. cylindrus/nana* during the POWELL-2020 campaign (Fig. 3b and 5) is consistent with previous reports that documented the dominance of this species in the southern Drake Passage and Weddell Sea (Kang and Fryxell, 1992; Kang and Fryxell, 1993; Cefarelli et al., 2010). Moreover, our results underscore the strong affinity of this species towards regions under the influence of sea ice, as previously reported in both water column and seafloor sediments (Leventer, 1992; Zielinski and Gersonde, 1997; Armand et al., 2005, among others). Likewise, the important contribution of *F. pseudonana* in the AAZ and SZ (Fig. 3b and 5), in both early January and late January-early February, is in agreement with previous research that reported this species as a major component of the diatom communities during summer in the Drake Passage (Kang and Lee, 1995; Cefarelli et al., 2010) and NW Elephant Island (the most northerly of the South Shetland Islands, Villafañe et al., 1995). This species has been also described as an important contributor of the diatom assemblages in the high-nutrient, low-chlorophyll (HNLC) waters off Kerguelen Archipelago (Armand et al., 2008) and as part of the

sinking diatom assemblages collected by sediment traps in AZ south of Tasmania (Rigual-Hernández et al., 2015), suggesting the capacity of this species to also thrive under low iron levels.

The low contribution of *Chaetoceros* RS in our survey contrasts with the high abundance of this taxon in the surface sediments of the Bransfield Strait (> 400 10⁶ valves g⁻¹ of dry sediment; Crosta et al., 1997). *Chaetoceros* RS formation has been related to nitrogen depletion and/or light limitation (Bodungen et al., 1986; Kuwata and Takahashi, 1990; Leventer, 1991). In particular, silicon to nitrate molar ratios above 9.3 have been documented to trigger resting spore formation in *Chaetoceros* populations (Kuwata and Takahashi, 1990). The only neritic stations (i.e. the habitat of the resting spore forming *Chaetoceros* subgenus *Hyalochaete*) with relatively high silicon to nitrogen ratios during our survey were those in the Bransfield Strait and Northern Weddell Sea with values ranging from 4.4 to 8.4. Despite these relatively high values, only in the stations South Bay of Livingston Island some *Chaetoceros* RS were registered in concentrations above 5%. Taken together, all the above indicate that the interplay of more environmental factors aside from nitrogen limitation (e.g. light limitation) are required to trigger *Chaetoceros* RS formation in the Bransfield Strait. It is likely that the moment of the sampling was too early or too late in the seasonal succession to capture the formation of resting spores by *Chaetoceros* populations in the neritic habitats of the Antarctic Peninsula (Leventer, 1991).

The co-occurrence of the epiphytic and sea-ice affiliated *P. kamtschaticum* (Medlin, 1990; Scott and Marchant, 2005; Majewska et al., 2015) with elevated concentrations of fine sediments in the coastal waters of Livingston Island, is a clear reflection of the affinity of this species for glacial meltwater discharge. It is important to note that the affinity of *P. kamtschaticum* for high salinities suggested by the CCA is considered an artifact caused by the exclusion of some stations with high contributions of this species near meltwater sources (owing to the lack of accompanying measurements of some environmental parameters, see methods section). Indeed, the geographical distribution of *P. kamtschaticum* during our survey suggests the potential of this species as proxy for glacial meltwater discharge in the paleorecord. Moreover, the co-occurrence of peak relative contribution of *Navicula* spp. in the same stations also indicates that this taxon was also associated to the sediment input from subglacial waters (Fig. 3e). However, the utility of *Navicula* as a proxy for glacial discharge should be made with caution as this genus contains species both benthic and planktonic species (Al-Handal and Wulff, 2008; Majewska et al., 2015; Rigual-Hernández et al., 2015; Daglio et al., 2018; Silva et al., 2019).

Lastly, although the resolution of our light microscopy analysis was not sufficient to resolve the identification of small centric diatoms (grouped here as small centric < $20 \, \mu m$ group; Fig. 3f), SEM analysis of selected samples indicate that, at least some of the specimens were *Minidiscus chilensis*. This species had been previously documented in large numbers in the western Bransfield Strait (Kang et al., 2003) and Ryder Bay (Annett et al., 2010). Owing to the relevant contribution of the small centric group in some samples during the POWELL-2020 expedition (Fig. 3f) and the potential relevant role of *Minidiscus* in the biological pump of the region (Leblanc et al., 2018), we recommend investing extra efforts in identifying small diatom species in future surveys in the AP.

In terms of coccolithophore distributions, the observed latitudinal pattern (i.e. coccolithophores were most abundant north of the PF) is consistent with previous reports in the Drake Passage and AP (Charalampopoulou et al., 2016; Saavedra-Pellitero et al., 2019) and in other sectors of the Southern Ocean (Cubillos et al., 2007; Malinverno et al., 2015; Saavedra-Pellitero and Baumann, 2015; Patil et al., 2017; Rigual Hernández et al., 2018; Trull et al., 2018;

Rigual-Hernández et al., 2020b, among others). The substantially lower cell numbers than those of diatoms, together with the small size of their coccospheres indicate that coccolithophores must account for only a small fraction of the algal biomass during our survey. This observation is consistent with previous studies where coccolithophore contribution to total phytoplankton biomass accumulation has been shown to be small, accounting for less than 10% in subantarctic waters and less than 1% in Antarctic waters (Trull et al., 2018). Among all the environmental parameters controlling coccolithophore distribution, temperature has been suggested to play a major role their latitudinal distribution in the Southern Ocean (Boyd et al., 2010; Feng et al., 2017; Rigual-Hernández et al., 2020a). Moreover, temperature also represents a major control for coccolithophore diversity (Rigual-Hernández et al., 2020b), with assemblages turning nearly or entirely monospecific south of the PF (Cubillos et al., 2007; Malinverno et al., 2015; Patil et al., 2017; Rigual Hernández et al., 2018; Saavedra-Pellitero et al., 2019).

4.2 Processes and implications on surface water properties of the 2020 marine heatwave

The 2020 MHW observed across the Drake Passage and AP offers valuable insight into the nuanced interplay between mesoscale ocean circulation and biogeochemical variability in the Southern Ocean. Our data reveal that this extreme event was neither solely a product of atmospheric forcing nor simply a reflection of long-term warming trends. Instead, the development and persistence of the 2020 MHW were closely tied to mesoscale anticyclonic eddy dynamics, as indicated by sustained positive SLA exceeding +20 cm along the northbound transect (Fig. 7a). Mesoscale eddy formation is characteristic of the Drake Passage, where the proximity of major circumpolar fronts enhances eddy activity relative to other sectors of the Southern Ocean (Rintoul et al., 1997; Beech et al., 2022), resulting in pronounced horizontal and vertical gradients in water properties.

The warm water anomaly recorded during the northbound transit of the POWELL-2020 campaign—immediately preceding the core of the heatwave—coincided with elevated SLA and increased ADT, classic markers of surface-intensified anticyclonic eddies. These features effectively trap heat, suppressing vertical mixing and allowing anomalously warm, stratified surface waters to persist. Our estimates of EKE and VIKE further support that these events were primarily confined to the upper ocean, with deeper kinetic energy redistribution occurring only after the MHW's peak (Fig. 7f). Satellite-derived SST anomalies revealed sustained surface warming of more than +3°C above climatological values, underscoring the spatial signature of these mesoscale structures.

The impact of mesoscale circulation on nutrient distribution was likewise significant. The advection of warm, low-nutrient waters from northern circumpolar regions—likely mediated by these eddies—resulted in exceptionally low nitrate and phosphate concentrations north of the Polar Front, reaching levels nearly an order of magnitude below typical summer values (Fig. 2b). South of the major fronts, the biogeochemical response was more nuanced: while nitrate and phosphate remained relatively high, silicate displayed steep meridional gradients, consistent with the established position of the silicate front. This spatial heterogeneity in nutrient availability appears to have governed the observed phytoplankton community composition and bloom dynamics. Comparable links between mesoscale circulation, MHWs and phytoplankton dynamics have been observed in other Antarctic sectors (Fernández-Barba et al., 2024; Frenger et al., 2018; Ma and Chen, 2025), underscoring the tight coupling between physics and biogeochemistry in these areas.

Analysis of the distribution and makeup of diatom communities provides further evidence of the origin of the 2020 marine heat wave in the Drake Passage. The presence of Chaetoceros resting spores from the SAZ to the AAZ during the northbound transit (Fig. 3d) supports the idea that the advection of an anticyclonic eddy from the northernmost systems of the Drake Passage was responsible for the anomalously high SSTs recorded during the northbound transit. This is because the habitat of Chaetoceros subgenus Hyalochaete is restricted to coastal and inshore waters (Hasle and Syvertsen, 1997), and therefore, the presence of resting spores of this taxon in pelagic environments can be taken as an indicator of influence of coastal settings (e.g. Lange et al., 1994; Treppke et al., 1996; Wilks et al., 2021). Likewise, it is possible that the remarkable increase in the relative abundance of *Thalassiosira* spp. documented in the SAZ during the northbound transit was also associated, or partially associated, with the transport of coastal diatom assemblages, which are often rich in species of the order Thalassiosirales (Ferrario et al., 2018), into the Southern Ocean. This idea is supported by previous observations of eddy and meander formation in the Subantarctic Zone and their subsequent transport across the Polar Front in the Southern Ocean in general (Hogg et al., 2008), and in the Drake Passage (Meredith and Hogg, 2006) and the Weddell-Scotia confluence (Kahru et al., 2007), in particular. It could be argued that the advected Chaetoceros RS and Thalassiosira spp., should have been accompanied by the transport of subantarctic coccolithophores south of the Polar Front. However, it should be noted Chaetoceros RS are highly resistant to degradation (e.g. Rembauville et al., 2016; Rembauville et al., 2018) while coccospheres disarticulate rapidly after cell death. Therefore, it is possible that the advected waters transported a signal of subantarctic coccolithophores but in the form of detached coccoliths, which were not assessed in the current study.

In summary, our findings demonstrate that the onset and maintenance of the 2020 MHW in the Drake Passage were driven primarily by internal oceanic processes—specifically, the activity of energetic anticyclonic eddies—rather than by direct atmospheric heat input. These eddy features not only structured the thermal characteristics of the upper ocean but also modulated the spatial distribution of key nutrients, fundamentally shaping the biogeochemical and ecological environment experienced by primary producers. A deeper understanding of the coupling between mesoscale circulation, nutrient fluxes, and biological responses is essential for predicting the sensitivity of Southern Ocean ecosystems in an era of rapid, dynamic warming.

4.3 Influence of the marine heat wave on phytoplankton communities and nutrient distributions

The MHW documented in the Drake Passage in late-January early-February was coupled with the development of a diatom bloom in the SZ and AAZ and substantial shifts in the relative contributions of major components of the diatom assemblage (Fig. 3). Additionally, significant changes in macronutrient distributions were observed throughout most of the Drake Passage as well as changes in coccolithophore distributions. These changes are examined in detail next.

The diatom bloom observed in the SZ and AAZ during the MHW reached cell concentrations of up to ca. 5.5×10^6 and 5×10^6 cells L⁻¹, respectively (Fig. 3a). These values were one to three orders of magnitude greater than previous reports in the same zonal systems during summer (Villafañe et al., 1995; Olguin et al., 2006; Cefarelli et al., 2010). The bloom was mainly composed of *F. cylindrus/nana* which exhibited an increase in both its relative (Fig. 6i) and absolute abundance. The positive effect of the warm water anomaly on the development of this taxon is supported by the incubation experiments by Antoni et al. (2020) who documented that warming has a positive effect on the growth rates of *F. cylindrus* while decreasing its iron

requirements (Jabre and Bertrand, 2020). The increase in the relative contribution of *F. cylindrus/nana* was also coupled with an increase in the absolute abundance of *F. pseudonana* (and a non-significant change in its relative contribution; Fig. 6j). This suggests that the warmer water conditions during the MHW stimulated the growth of *F. pseudonana* although to a lower extent than for *F. cylindrus/nana*. In turn, the significant decrease in the relative contribution of the larger *F. kerguelensis* in the southern Drake Passage suggests a poorer tolerance of this species to warm water anomalies than its small-sized counterparts.

It is important to note that the diatom bloom in the SZ and AAZ was not coupled with a significant change in the chlorophyll-a concentration - as suggested by the fluorescence - or in the net primary productivity (Fig. 6f and 6g, respectively). This mismatch with the increase in diatom cell abundance can be attributed to several factors. Firstly, other phytoplankton functional groups (e.g. cryptophytes and prymnesiophytes) can contribute substantially to the total chlorophyll-a production in the study region (Moline et al., 2004; Montes-Hugo et al., 2008). Therefore, changes in the relative contribution of these groups throughout our survey could have contributed to the lack of a clear relationship between diatom cell numbers, fluorescence and NPP. Secondly, diatom assemblages display a wide range of sizes with cellular biovolumes spanning up to over nine orders of magnitude in the world ocean (Leblanc et al., 2012). Therefore, a shift in the proportions of the dominant diatom species does not necessarily imply a proportional change in the chlorophyll-a signal, as the amount of chlorophyll-a content across species may vary substantially (Chan, 1978). Thirdly, variations in NPP do not always directly reflect phytoplankton biomass, particularly in Southern Ocean environments that are co-limited by nutrients and light. In these areas, phytoplankton can adjust their C:Chl-a cellular ratios in response to transient climatic events such as MHWs (Behrenfeld et al., 2016). This physiological plasticity is further modulated by light availability, which in the Southern Ocean is strongly influenced by persistent cloud cover; under such conditions, phytoplankton adjust their pigmentation through photoacclimation, with important consequences for NPP estimates (Begouen Demeaux et al., 2025).

It should be noted that although our evidence suggests that the relationship between the occurrence of the MHW and the diatom bloom in the southern Drake Passage is causative, it could be argued that the enhanced diatom abundance between early January and late January may be the result of the regular seasonal progression of diatom productivity. Chlorophyll-a climatology (years 1998-2022) for the southern Drake Passage estimated by Ferreira et al. (2024) indicates that average algal biomass accumulation between early January and early February almost did not change (less than 0.1 mg Chl-a m⁻³ difference between them). Assuming a similar relative contribution of diatoms to the total Chl-a signal between January and February, a similar diatom abundance concentration could be expected in early January and in early February during a regular year. It follows that the enhanced abundance in diatom concentrations documented during the northbound transit was most likely the result of an exceptional event rather than the regular phenological response of diatoms in this region.

Aside from the above-mentioned diatom bloom in the southern Drake Passage, the onset of the MHW was associated with a pronounced and significative drawdown in nitrate concentrations and a reduction of phosphate concentrations in a large portion of the Drake Passage (Fig. 2b, 6c and 6d). We interpret the anomalously low nitrate and phosphate concentrations to result from limited vertical nutrient supply to the euphotic zone induced by warming together with a steady consumption of nutrients by phytoplankton. This hypothesis is supported by previous work that described that anomalous warming events, such as MHWs,

generally drive a reduction of mixed layer depths (Amaya et al., 2021; Oliver et al., 2021) and widespread surface nutrient declines in subpolar and polar ecosystems (e.g. Peña et al., 2019; Servettaz et al., 2025). However, aside from a reduction of nutrient supply, enhanced nutrient consumption by phytoplankton would be required to explain the unusually low nitrate concentrations observed during the northbound transit (Fig. 2 and Table 1). The development of the diatom bloom to the south of the Polar Front might have been responsible, or significantly contributed, to the nutrient depletion. This notion is in agreement with some studies in the Antarctic Peninsula where anomalously low nitrate concentrations (below 5 μM L-1) had been reported associated with the development of intense phytoplankton blooms (Holm-Hansen et al., 1989; Karl et al., 1991; Servettaz et al., 2025). However, the lack of a significant reduction in silicate concentration associated with the diatom bloom south of the PF (Fig. 2b and 6e) may seem puzzling at first. Looking in detail into the makeup of the diatom assemblage gives us some hints to reconcile these results. As mentioned, previously, the main components of the diatom bloom were small Fragilariopsis species (e.g. the apical axis length of F. nana is 3-10 µm length in our study region; Cefarelli et al., 2010) that are characterized with a substantially lower silica requirement than larger, robustly silicified diatoms such as F. kerquelensis (apical length ranging from 17 to 83 µm; Cefarelli et al., 2010). This feature, together with the rapid silicate recycling of the frustules of small Fragilariopsis species in the upper water column (Grigorov et al., 2014; Rigual-Hernández et al., 2016) appear to be sufficient to sustain high diatom cell concentrations without a remarkable silica consumption.

855

856

857

858

859

860

861

862

863

864

865

866

867

868

869

870

871

872

873

874

875

876

877

878

879

880 881

882

883

884

885

886

887

888

889

890

891

892

893

894

895

896

897

898

899

900

901

Regarding the coccolithophore response, it is worth noting that average coccolithophore abundance decreased two-fold in the SAZ and PFZ during the MHW compared with the observations made in the southbound transit (Fig. 4) even though no statistical difference was found between both the southbound and northbound transits (Fig. 6I). Notably, coccolithophore concentrations were also substantially lower than previous reports during the austral summer in both the SAZ (23 x 10⁴ coccospheres L⁻¹, Charalampopoulou et al. 2016; 15 x 10⁴ coccospheres L⁻ 1 , Saavedra-Pellitero et al. 2019) and PFZ (58 x 10^{4} coccospheres L $^{ ext{-}1}$, Charalampopoulou et al. 2016; 11×10^4 coccospheres L⁻¹, Saavedra-Pellitero et al. 2019). Therefore, it could be speculated that the warm water anomaly may be responsible for the low coccolithophore productivity. As mentioned before, both laboratory experiments (Feng et al., 2017) and field evidence (Rivero-Calle et al., 2015) have underscored the primary role of temperature in the control of coccolithophore growth rates. However, according to these studies, an increase of SSTs would imply an increase of growth rates, which is opposite to what we observed during the POWELL-2020 campaign. It follows that different environmental controls other than temperature must have been responsible for the decrease in coccolithophore abundance within the SAZ and PFZ. Notably, Trull et al. (2018) indicated that macronutrient availability could be an important factor determining the growth of coccolithophores in oligotrophic waters at the northern edge of the Southern Ocean. This idea is reinforced by laboratory culture experiments that revealed that nitrate concentration is a critical factor controlling the photosynthetic and growth rates of subantarctic E. huxleyi (Feng et al., 2017). The latter study also demonstrated that, in contrast to nitrate, the growth rate of E. huxleyi remained relatively constant across a wide range of phosphate concentrations. Taking into consideration all the above, it is possible that the drop of ca. one order of magnitude of nitrate concentrations during the northbound transit could have been responsible for low coccolithophore abundance. However, it should be acknowledged that this interpretation remains speculative and there are of course other possible explanations for the low coccolithophore cell numbers, including zooplankton grazing control, which was not assessed in our survey. Lastly, our data also suggests the change in nutrient concentrations

and/or warming induced by the warm water anomaly favoured the development of *C. leptoporus* over *E. huxleyi* that is a good competitor for phosphate, but does not grow well under low nitrate levels (Egge and Heimdal, 1994).

902

903

904

905

906

907

908

909

910

911

912

913

914

915

916

917

918

919

920

921

922

923

924

925

926

927

928

929

930

931

932

933

934

935

936

937

938

939

940

941

942

943

944

945

946

947

Before extrapolating our results into a broader context, it is important to acknowledge the limitations of our study, including the discrete sampling of the water column before and during the MHW. Multi-day monitoring of the water column in the areas affected by the MHW would be required to evaluate the evolution of phytoplankton communities through time (e.g. Landry et al., 2024). Also, it should be acknowledged that the current study only provides evidence of the response of phytoplankton assemblages in the surface layer (i.e. 5 m depth), but it is possible that phytoplankton communities below the surface mixed layer may have responded differently to the MHW. Moreover, our study focussed on two major phytoplankton groups, but to be able to evaluate shifts in the phytoplankton community future studies should also address other relevant algal groups, including important soft-tissue phytoplankton, such as, cryptophytes and *Phaeocystis*. Identification and quantification of chlorophyll-a and marker pigments of the main phytoplankton taxonomic groups would also complement microscopybased methods providing a more robust picture of the response of phytoplankton communities to MHWs. Despite these limitations, our results tentatively suggest that an increase in the frequency of warm water anomalies could potentially favour the development of small diatom species in the southern circumpolar systems of the Southern Ocean and a decrease in coccolithophore numbers north of the PF. However, owing to low contribution of coccolithophore communities to phytoplankton biomass and their mild response to the warming event, it is likely that a moderate decrease in coccolithophore numbers does not represent a major impact for trophic chain or the biogeochemical cycles in the low productivity ecosystems where they thrive (i.e. mainly SAZ and PFZ). In turn, the more pronounced shifts in the abundance and composition of diatom communities, which often dominate algal biomass accumulation in the most productive ecosystems of Antarctica, are likely to be far reaching. An increase in the abundance of small diatom species is in agreement with in situ and model observations that indicate that warm water anomalies will result in an increasing importance of small size phytoplankton in the world's oceans (Acevedo-Trejos et al., 2014; Peña et al., 2019; Wyatt et al., 2022). This shift in the composition and average size reduction of phytoplankton communities may result in impacts in the food chain and efficiency of the biological pump. Previous studies indicate that an average reduction in the cell size of phytoplankton communities in the Antarctic Ocean could have important impact on the abundance of keystone zooplankton grazers, particularly salps and krill (Moline et al., 2008). Since krill feed mainly on phytoplankton cells larger than 10 µm, the overall size reduction of phytoplankton communities has resulted in a decrease of krill numbers and an increase in salp abundance (grazers unaffected by the size of their prey) (Moline et al., 2008). Because krill represents the primarily food source for many Antarctic birds and mammals (Atkinson et al., 2004), a shift in the phytoplankton communities, and therefore krill abundance, is predicted to have a substantial negative effect on the krilldependent food chain (Murphy et al., 2007, 2016). The possible implications in the efficiency of the biological pump are less clear. While small diatom are traditionally regarded as less efficient carbon vectors to the deep ocean than larger diatoms owing to their faster remineralization in the upper water column (e.g. Legendre and Le Fèvre, 1995), some studies have challenged this view. Leblanc et al. (2018) demonstrated that small-sized diatoms (2-20 μm) can develop large blooms across the global ocean (including the Antarctic Peninsula) and reach the seafloor at high sinking rates, thereby contributing substantially to carbon sequestration. Therefore, the impact

of an increase in the abundance of small size diatoms species in carbon sequestration in the Southern Ocean is still uncertain and remain to be quantified and parameterized.

Conclusions

948

949

950

951 952

953

954

955

956

957

958

959

960

961

962

963

964

965

966

967

968

969

970

971

972

973

975

976

977

978

979

980

981

982

983

984

985

986

Our evidence, albeit circumstantial, suggests that extreme warming events in southernmost circumpolar systems of the Drake Passage can be driven by the advection of mesoscale anticyclonic eddies from lower latitudes. Notably, the unusually warmer conditions generated by these eddies can drive substantial changes in the abundance and structure of phytoplankton communities. Our results provide field-based evidence for observations made on culture experiments that indicate that the growth of small Fragilariopsis species is stimulated by warmer water temperatures. The remarkable nitrate drawdown observed in large swath of the Drake during the onset of the MHW indirectly suggests that warm water anomalies may favour the development of soft-tissue phytoplankton in the Drake Passage. Moreover, it is likely that the low nitrate levels resulted in a reduction of coccolithophore productivity north of the PF. As both the intensity and frequency of warm water anomalies are expected to increase in the Southern Ocean in the coming decades, an increase in the abundance smaller diatom taxa could be expected. This shift in the phytoplankton community structure, will most likely have an impact on higher trophic levels, particularly krill and salps, ultimately affecting higher trophic levels as well as the functioning of the marine carbon cycle. While our study has provided valuable insights into the intricate relationship between Antarctic phytoplankton and environmental change, it is evident that further research is required to fully comprehend their complex response. This requires regular monitoring of key Southern Ocean regions to identify shifts in phytoplankton composition and structure under extreme climatic conditions like MHW. Achieving this ambitious goal will require international cooperation and data sharing among nations (e.g. ICEPRO working group; Etourneau et al., 2025), as no single country can accomplish it alone.

Data availability

All data presented in the figures can be found in the supplement files.

Author contributions

CE, FJJ and FB planned and led the POWELL-2020 campaign. The conceptualization of the manuscript was primarily done by ARH, MAB, JAF and AL. AL, JAF, DE and JE performed the water sampling. MFB and GN obtained and interpreted satellite and modelled data. ARH, AL and JAF led the phytoplankton study. ARH, AL, MD and MAB performed the sample processing, microscopy and image analyses for characterization and quantification of the diatom assemblage. ARH and JAF performed microscopy analysis for the characterization and quantification of the coccolithophore assemblage. JE and MS performed nutrient analyses. JMSS and ARH performed statistical analyses. Manuscript writing was led by ARH with substantial contributions and edits by MFB, GN and AL. All authors contributed to the interpretation of the data, manuscript review and editing. We thank our reviewers for their close reading of the manuscript and their comments that helped to improve the manuscript substantially.

987

988

989

990

Acknowledgements

ARH and MAB acknowledge funding from project BASELINE (PID2021- 126495NB-741 C33) funded by the Spanish MCIN/AEI/10.13039/5011000110 33. CE and FB acknowledge funding

- 991 from the AntOCEAN project PID2021- 126495NB-741 C31/C32 cofounded by the European
- 992 Union through FEDER funds. DE was funded by the UK Research and Innovation Engineering and
- 993 Physical Sciences Research Council (grant number EP/X02623X/1). Authors would like to thank
- the BIO-Hespérides captain and crew and the UTM personnel for their hard work and technical
- assistance during the cruise. Authors wish to thank Ms Jane Carskaddan and Mr Zach O'Donnell
- 996 (Colgate University) for assistance with scanning electron microscopy analyses and Julia
- 997 Gutiérrez-Pastor for her assistance with water sampling. The authors thank all members of the
- 998 Copernicus Marine Service, the Copernicus Climate Change Service, and the ECMWF for
- 999 providing satellite-derived and modelled data essential to this work. We thank GEBCO for the
- 1000 GEBCO Grid 2024 used as background for map in figure 1. We thank our reviewers for their close
- reading of the manuscript and their comments.

References

1002

- 1003 Acevedo-Trejos, E., Brandt, G., Steinacher, M., and Merico, A.: A glimpse into the future
- 1004 composition of marine phytoplankton communities, Frontiers in Marine Science, 1,
- 1005 10.3389/fmars.2014.00015, 2014.
- 1006 Al-Handal, A. Y., and Wulff, A.: Marine epiphytic diatoms from the shallow sublittoral zone
- in Potter Cove, King George Island, Antarctica, 2008.
- 1008 Amaya, D. J., Alexander, M. A., Capotondi, A., Deser, C., Karnauskas, K. B., Miller, A. J., and
- 1009 Mantua, N. J.: Are long-term changes in mixed layer depth influencing North Pacific marine
- heatwaves?, Bulletin of the American Meteorological Society, 102, S59-S66, 2021.
- 1011 Aminot, A., Kérouel, R., and Coverly, S. C.: Nutrients in seawater using segmented flow
- analysis, in: Practical guidelines for the analysis of seawater, CRC press, 143-178, 2009.
- 1013 Annett, A. L., Carson, D. S., Crosta, X., Clarke, A., and Ganeshram, R. S.: Seasonal
- 1014 progression of diatom assemblages in surface waters of Ryder Bay, Antarctica, Polar Biol,
- 1015 33, 13-29, 10.1007/s00300-009-0681-7, 2010.
- 1016 Annett, A. L., Fitzsimmons, J. N., Séguret, M. J. M., Lagerström, M., Meredith, M. P.,
- 1017 Schofield, O., and Sherrell, R. M.: Controls on dissolved and particulate iron distributions
- in surface waters of the Western Antarctic Peninsula shelf, Marine Chemistry, 196, 81-97,
- 1019 https://doi.org/10.1016/j.marchem.2017.06.004, 2017.
- 1020 Antoni, J. S., Almandoz, G. O., Ferrario, M. E., Hernando, M. P., Varela, D. E., Rozema, P. D.,
- Buma, A. G., Paparazzo, F. E., and Schloss, I. R.: Response of a natural Antarctic
- 1022 phytoplankton assemblage to changes in temperature and salinity, Journal of
- 1023 Experimental Marine Biology and Ecology, 532, 151444, 2020.
- 1024 Ardelan, M. V., Holm-Hansen, O., Hewes, C. D., Reiss, C. S., Silva, N. S., Dulaiova, H.,
- 1025 Steinnes, E., and Sakshaug, E.: Natural iron enrichment around the Antarctic Peninsula in
- 1026 the Southern Ocean, Biogeosciences, 7, 11-25, 10.5194/bg-7-11-2010, 2010.
- 1027 Armand, L. K., Crosta, X., Romero, O., and Pichon, J.-J.: The biogeography of major diatom
- 1028 taxa in Southern Ocean sediments: 1. Sea ice related species, Palaeogeography,
- 1029 Palaeoclimatology, Palaeoecology, 223, 93-126,
- 1030 http://dx.doi.org/10.1016/j.palaeo.2005.02.015, 2005.
- 1031 Armand, L. K., Cornet-Barthaux, V., Mosseri, J., and Quéguiner, B.: Late summer diatom
- 1032 biomass and community structure on and around the naturally iron-fertilised Kerguelen
- 1033 Plateau in the Southern Ocean, Deep Sea Research Part II: Topical Studies in
- 1034 Oceanography, 55, 653-676, http://dx.doi.org/10.1016/j.dsr2.2007.12.031, 2008.
- 1035 Assmy, P., Smetacek, V., Montresor, M., Klaas, C., Henjes, J., Strass, V. H., Arrieta, J. M.,
- 1036 Bathmann, U., Berg, G. M., Breitbarth, E., Cisewski, B., Friedrichs, L., Fuchs, N., Herndl, G.
- J., Jansen, S., Krägefsky, S., Latasa, M., Peeken, I., Röttgers, R., Scharek, R., Schüller, S. E.,
- 1038 Steigenberger, S., Webb, A., and Wolf-Gladrow, D.: Thick-shelled, grazer-protected
- 1039 diatoms decouple ocean carbon and silicon cycles in the iron-limited Antarctic

- 1040 Circumpolar Current, Proceedings of the National Academy of Sciences, 110, 20633-
- 1041 20638, 10.1073/pnas.1309345110, 2013.
- 1042 Atkinson, A., Siegel, V., Pakhomov, E., and Rothery, P.: Long-term decline in krill stock and
- increase in salps within the Southern Ocean, Nature, 432, 100-103, 2004.
- Ballerini, T., Hofmann, E. E., Ainley, D. G., Daly, K., Marrari, M., Ribic, C. A., Smith Jr, W. O.,
- 1045 and Steele, J. H.: Productivity and linkages of the food web of the southern region of the
- 1046 western Antarctic Peninsula continental shelf, Progress in Oceanography, 122, 10-29,
- 1047 2014.
- 1048 Beech, N., Rackow, T., Semmler, T., Danilov, S., Wang, Q., and Jung, T.: Long-term
- 1049 evolution of ocean eddy activity in a warming world, Nature Climate Change, 12, 910-917,
- 1050 10.1038/s41558-022-01478-3, 2022.
- 1051 Begouen Demeaux, C., Boss, E., Graff, J. R., Behrenfeld, M. J., and Westberry, T. K.:
- 1052 Phytoplanktonic Photoacclimation Under Clouds, Geophysical Research Letters, 52,
- 1053 e2024GL112274, https://doi.org/10.1029/2024GL112274, 2025.
- 1054 Behrenfeld, M. J., O'Malley, R. T., Boss, E. S., Westberry, T. K., Graff, J. R., Halsey, K. H.,
- 1055 Milligan, A. J., Siegel, D. A., and Brown, M. B.: Revaluating ocean warming impacts on
- 1056 global phytoplankton, Nature Climate Change, 6, 323-330, 2016.
- 1057 Bell, J. J., Micaroni, V., Strano, F., Ryan, K. G., Mitchell, K., Mitchell, P., Wilkinson, S.,
- 1058 Thomas, T., Bachtiar, R., and Smith, R. O.: Marine heatwave-driven mass mortality and
- 1059 microbial community reorganisation in an ecologically important temperate sponge,
- 1060 Global change biology, 30, e17417, 2024.
- 1061 Bendschneider, K., and Robinson, R. J.: A new spectrophotometric method for the
- determination of nitrite in sea water, 1952.
- 1063 Bertolin, M. L., and Schloss, I. R.: Phytoplankton production after the collapse of the
- 1064 Larsen A Ice Shelf, Antarctica, Polar Biol, 32, 1435-1446, 2009.
- 1065 Bian, C., Jing, Z., Wang, H., Wu, L., Chen, Z., Gan, B., and Yang, H.: Oceanic mesoscale
- 1066 eddies as crucial drivers of global marine heatwaves, Nature Communications, 14, 2970,
- 1067 10.1038/s41467-023-38811-z, 2023.
- 1068 Blanchard-Wrigglesworth, E., Roach, L. A., Donohoe, A., and Ding, Q.: Impact of Winds
- 1069 and Southern Ocean SSTs on Antarctic Sea Ice Trends and Variability, Journal of Climate,
- 1070 34, 949-965, https://doi.org/10.1175/JCLI-D-20-0386.1, 2021.
- 1071 Bodungen, B. v., Smetacek, V. S., Tilzer, M. M., and Zeitzschel, B.: Primary production and
- 1072 sedimentation during spring in the Antarctic Peninsula region, Deep Sea Research Part A.
- 1073 Oceanographic Research Papers, 33, 177-194, 1986.
- Bond, N. A., Cronin, M. F., Freeland, H., and Mantua, N.: Causes and impacts of the 2014
- warm anomaly in the NE Pacific, Geophysical Research Letters, 42, 3414-3420,
- 1076 https://doi.org/10.1002/2015GL063306, 2015.
- 1077 Boyd, P., and Trull, T.: Understanding the export of biogenic particles in oceanic waters: Is
- there consensus?, Progress in Oceanography, 72, 276-312, 2007.
- 1079 Boyd, P. W., Strzepek, R., Fu, F., and Hutchins, D. A.: Environmental control of open-ocean
- 1080 phytoplankton groups: Now and in the future, Limnology and Oceanography, 55, 1353-
- 1081 1376, 10.4319/lo.2010.55.3.1353, 2010.
- 1082 Cavole, L. M., Demko, A. M., Diner, R. E., Giddings, A., Koester, I., Pagniello, C. M., Paulsen,
- 1083 M.-L., Ramirez-Valdez, A., Schwenck, S. M., and Yen, N. K.: Biological impacts of the 2013-
- 1084 2015 warm-water anomaly in the Northeast Pacific: winners, losers, and the future,
- 1085 Oceanography, 29, 273-285, 2016.
- 1086 Cefarelli, A. O., Ferrario, M. E., Almandoz, G. O., Atencio, A. G., Akselman, R., and Vernet,
- 1087 M.: Diversity of the diatom genus Fragilariopsis in the Argentine Sea and Antarctic waters:
- 1088 morphology, distribution and abundance, Polar Biol, 33, 1463-1484, 10.1007/s00300-010-
- 1089 0794-z, 2010.
- 1090 Chan, A. T.: COMPARATIVE PHYSIOLOGICAL STUDY OF MARINE DIATOMS AND
- 1091 DINOFLAGELLATES IN RELATION TO IRRADIANCE AND CELL SIZE. I. GROWTH UNDER

- 1092 CONTINUOUS LIGHT, Journal of Phycology, 14, 396-402, https://doi.org/10.1111/j.1529-
- 1093 <u>8817.1978.tb02458.x</u>, 1978.
- 1094 Charalampopoulou, A., Poulton, A. J., Bakker, D. C., Lucas, M. I., Stinchcombe, M. C., and
- 1095 Tyrrell, T. J. B.: Environmental drivers of coccolithophore abundance and calcification
- 1096 across Drake Passage (Southern Ocean), 13, 5917-5935, 2016.
- 1097 Cook, A., Fox, A., Vaughan, D., and Ferrigno, J.: Retreating glacier fronts on the Antarctic
- 1098 Peninsula over the past half-century, Science, 308, 541-544, 2005.
- 1099 Crosta, X., Pichon, J.-J., and Labracherie, M.: Distribution of Chaetoceros resting spores in
- 1100 modern peri-Antarctic sediments, Marine Micropaleontology, 29, 283-299, 1997.
- 1101 Cubillos, J., Wright, S., Nash, G., De Salas, M., Griffiths, B., Tilbrook, B., Poisson, A., and
- 1102 Hallegraeff, G.: Calcification morphotypes of the coccolithophorid *Emiliania huxleyi* in the
- 1103 Southern Ocean: changes in 2001 to 2006 compared to historical data, Marine Ecology
- 1104 Progress Series, 348, 47-54, 2007.
- 1105 Daglio, Y., Sacristán, H., Ansaldo, M., and Rodríguez, M. C.: Benthic diatoms from Potter
- 1106 Cove, 25 de Mayo (King George) Island, Antarctica: Mucilage and glucan storage as a C-
- 1107 source for limpets, Polar Science, 15, 39-48, https://doi.org/10.1016/j.polar.2018.01.004,
- 1108 2018.
- 1109 Davison, B. J., Hogg, A. E., Moffat, C., Meredith, M. P., and Wallis, B. J.: Widespread
- increase in discharge from west Antarctic Peninsula glaciers since 2018, The Cryosphere,
- 1111 18, 3237-3251, 2024.
- 1112 Deppeler, S. L., and Davidson, A. T.: Southern Ocean Phytoplankton in a Changing
- 1113 Climate, Frontiers in Marine Science, 4, 10.3389/fmars.2017.00040, 2017.
- 1114 Eakin, C. M., Sweatman, H. P., and Brainard, R. E.: The 2014–2017 global-scale coral
- 1115 bleaching event: insights and impacts, Coral Reefs, 38, 539-545, 2019.
- 1116 Eayrs, C., Holland, D., Francis, D., Wagner, T., Kumar, R., and Li, X.: Understanding the
- 1117 Seasonal Cycle of Antarctic Sea Ice Extent in the Context of Longer-Term Variability,
- 1118 Reviews of Geophysics, 57, 1037-1064, https://doi.org/10.1029/2018RG000631, 2019.
- 1119 Egge, J. K., and Heimdal, B. R.: Blooms of phytoplankton including Emiliania huxleyi
- 1120 (Haptophyta). Effects of nutrient supply in different N: P ratios, Sarsia, 79, 333-348,
- 1121 10.1080/00364827.1994.10413565, 1994.
- 1122 Eppley, R.: Temperature and phytoplankton growth in the sea, Fishery Bulletin, 70, 1063-
- 1123 1085, 1972.
- 1124 Etourneau, J., Evangelinos, D., Escutia, C., Amrbrecht, L., Leventer, A., Duncan, B., Müller,
- 1125 J., Mohan, R., Tiwari, M., Dunbar, R. B., Cortese, G., Ikehara, M., McClymont, E., de Santis,
- 1126 L., Allen, C., Huang, X., Rigual-Hernández, A. S., Levy, R., and ICEPRO, S. A. G.: The SCAR
- 1127 ICEPRO Action Group: an international collaboration effort for improving paleoclimate
- research in the Southern Ocean, EGU General Assembly 2025, Vienna, 2025.
- 1129 Feng, Y., Roleda, M. Y., Armstrong, E., Boyd, P. W., and Hurd, C. L.: Environmental controls
- on the growth, photosynthetic and calcification rates of a Southern Hemisphere strain of
- the coccolithophore *Emiliania huxleyi*, Limnology and Oceanography, 62, 519-540,
- 1132 10.1002/lno.10442, 2017.
- 1133 Fernández-Barba, M., Belyaev, O., Huertas, I. E., and Navarro, G.: Marine heatwaves in a
- 1134 shifting Southern Ocean induce dynamical changes in primary production,
- 1135 Communications Earth & Environment, 5, 404, 2024.
- 1136 Ferrario, M. E., Almandoz, G. O., Cefarelli, A. O., Beszteri, B., Akselman, R., Fabro, E., and
- 1137 Cembella, A.: Shionodiscus gaarderae sp. nov. (Thalassiosirales, Thalassiosiraceae), a
- 1138 bloom-producing diatom from the southwestern Atlantic Ocean, and emendation of
- 1139 Shionodiscus bioculatus var. bioculatus, Diatom Research, 33, 25-37,
- 1140 10.1080/0269249X.2017.1423112, 2018.
- 1141 Ferreira, A., Mendes, C. R., Costa, R. R., Brotas, V., Tavano, V. M., Guerreiro, C. V., Secchi,
- 1142 E. R., and Brito, A. C.: Climate change is associated with higher phytoplankton biomass

- and longer blooms in the West Antarctic Peninsula, Nature Communications, 15, 6536,
- 1144 2024.
- 1145 Freeman, N. M., Munro, D. R., Sprintall, J., Mazloff, M. R., Purkey, S., Rosso, I., DeRanek, C.
- 1146 A., and Sweeney, C.: The observed seasonal cycle of macronutrients in Drake Passage:
- 1147 Relationship to fronts and utility as a model metric, Journal of Geophysical Research:
- 1148 Oceans, 124, 4763-4783, 2019.
- 1149 Frölicher, T. L., Fischer, E. M., and Gruber, N.: Marine heatwaves under global warming,
- 1150 Nature, 560, 360-364, 10.1038/s41586-018-0383-9, 2018.
- 1151 Froneman, P. W., Perissinotto, R., McQuaid, C. D., and Laubscher, R. K.: Summer
- 1152 distribution of netphytoplankton in the Atlantic sector of the Southern Ocean, Polar Biol,
- 1153 15, 77-84, 10.1007/BF00241045, 1995.
- 1154 Gao, G., Zhao, X., Jiang, M., and Gao, L.: Impacts of marine heatwaves on algal structure
- and carbon sequestration in conjunction with ocean warming and acidification, Frontiers
- 1156 in Marine Science, 8, 758651, 2021.
- 1157 Garrabou, J., Gómez-Gras, D., Medrano, A., Cerrano, C., Ponti, M., Schlegel, R.,
- 1158 Bensoussan, N., Turicchia, E., Sini, M., Gerovasileiou, V., Teixido, N., Mirasole, A.,
- 1159 Tamburello, L., Cebrian, E., Rilov, G., Ledoux, J.-B., Souissi, J. B., Khamassi, F., Ghanem,
- 1160 R., Benabdi, M., Grimes, S., Ocaña, O., Bazairi, H., Hereu, B., Linares, C., Kersting, D. K., la
- Rovira, G., Ortega, J., Casals, D., Pagès-Escolà, M., Margarit, N., Capdevila, P., Verdura, J.,
- 1162 Ramos, A., Izquierdo, A., Barbera, C., Rubio-Portillo, E., Anton, I., López-Sendino, P., Díaz,
- D., Vázquez-Luis, M., Duarte, C., Marbà, N., Aspillaga, E., Espinosa, F., Grech, D., Guala, I.,
- Azzurro, E., Farina, S., Cristina Gambi, M., Chimienti, G., Montefalcone, M., Azzola, A.,
- 1165 Mantas, T. P., Fraschetti, S., Ceccherelli, G., Kipson, S., Bakran-Petricioli, T., Petricioli, D.,
- 1166 Jimenez, C., Katsanevakis, S., Kizilkaya, I. T., Kizilkaya, Z., Sartoretto, S., Elodie, R., Ruitton,
- 1167 S., Comeau, S., Gattuso, J.-P., and Harmelin, J.-G.: Marine heatwaves drive recurrent mass
- 1168 mortalities in the Mediterranean Sea, Global Change Biology, 28, 5708-5725,
- 1169 https://doi.org/10.1111/gcb.16301, 2022.
- 1170 Gorodetskaya, I. V., Durán-Alarcón, C., González-Herrero, S., Clem, K. R., Zou, X., Rowe,
- 1171 P., Rodriguez Imazio, P., Campos, D., Leroy-Dos Santos, C., Dutrievoz, N., Wille, J. D.,
- 1172 Chyhareva, A., Favier, V., Blanchet, J., Pohl, B., Cordero, R. R., Park, S.-J., Colwell, S.,
- 1173 Lazzara, M. A., Carrasco, J., Gulisano, A. M., Krakovska, S., Ralph, F. M., Dethinne, T., and
- 1174 Picard, G.: Record-high Antarctic Peninsula temperatures and surface melt in February
- 1175 2022: a compound event with an intense atmospheric river, npj Climate and Atmospheric
- 1176 Science, 6, 202, 10.1038/s41612-023-00529-6, 2023.
- 1177 Gossart, A., Helsen, S., Lenaerts, J., Broucke, S. V., Van Lipzig, N., and Souverijns, N.: An
- 1178 evaluation of surface climatology in state-of-the-art reanalyses over the Antarctic Ice
- 1179 Sheet, Journal of Climate, 32, 6899-6915, 2019.
- 1180 Green, J., Heimdal, B., Paasche, E., and Moate, R.: Changes in calcification and the
- 1181 dimensions of coccoliths of Emiliania huxleyi (Haptophyta) grown at reduced salinities,
- 1182 Phycologia, 37, 121-131, 1998.
- 1183 Grigorov, I., Rigual-Hernandez, A. S., Honjo, S., Kemp, A. E. S., and Armand, L. K.: Settling
- 1184 fluxes of diatoms to the interior of the antarctic circumpolar current along 170°W, Deep
- 1185 Sea Research Part I: Oceanographic Research Papers, 93, 1-13,
- 1186 http://dx.doi.org/10.1016/j.dsr.2014.07.008, 2014.
- 1187 Gutierrez-Villanueva, M. O., Chereskin, T. K., and Sprintall, J.: Upper-ocean eddy heat flux
- 1188 across the Antarctic Circumpolar Current in Drake Passage from observations: Time-mean
- and seasonal variability, Journal of Physical Oceanography, 50, 2507-2527, 2020.
- Hasle, G. R., and Syvertsen, E. E.: Marine diatoms, Identifying marine phytoplankton.
- 1191 Academic Press, San Diego, CA, 5–385, 1997.
- Hayashida, H., Matear, R. J., and Strutton, P. G.: Background nutrient concentration
- 1193 determines phytoplankton bloom response to marine heatwaves, Global Change Biology,
- 1194 26, 4800-4811, https://doi.org/10.1111/gcb.15255, 2020.

- He, Q., Zhan, W., Feng, M., Gong, Y., Cai, S., and Zhan, H.: Common occurrences of
- 1196 subsurface heatwaves and cold spells in ocean eddies, Nature, 1-7, 2024.
- Hobday, A. J., Alexander, L. V., Perkins, S. E., Smale, D. A., Straub, S. C., Oliver, E. C.,
- 1198 Benthuysen, J. A., Burrows, M. T., Donat, M. G., and Feng, M.: A hierarchical approach to
- 1199 defining marine heatwaves, Progress in oceanography, 141, 227-238, 2016.
- 1200 Hobday, A. J., Oliver, E. C., Gupta, A. S., Benthuysen, J. A., Burrows, M. T., Donat, M. G.,
- 1201 Holbrook, N. J., Moore, P. J., Thomsen, M. S., and Wernberg, T.: Categorizing and naming
- 1202 marine heatwaves, Oceanography, 31, 162-173, 2018.
- Hogg, A. M. C., Meredith, M. P., Blundell, J. R., and Wilson, C.: Eddy Heat Flux in the
- 1204 Southern Ocean: Response to Variable Wind Forcing, Journal of Climate, 21, 608-620,
- 1205 https://doi.org/10.1175/2007JCLI1925.1, 2008.
- Holbrook, N. J., Scannell, H. A., Sen Gupta, A., Benthuysen, J. A., Feng, M., Oliver, E. C. J.,
- 1207 Alexander, L. V., Burrows, M. T., Donat, M. G., Hobday, A. J., Moore, P. J., Perkins-
- 1208 Kirkpatrick, S. E., Smale, D. A., Straub, S. C., and Wernberg, T.: A global assessment of
- marine heatwaves and their drivers, Nature Communications, 10, 2624, 10.1038/s41467-
- 1210 019-10206-z, 2019.
- Holm-Hansen, O., Mitchell, B. G., Hewes, C. D., and Karl, D. M.: Phytoplankton blooms in
- the vicinity of Palmer Station, Antarctica, Polar Biol, 10, 49-57, 1989.
- 1213 Isla, E., Menschel, E., and González, H. H.: Intense autumnal coastal biogenic particle
- 1214 settling fluxes align with phytoplankton phenology changes off the western Antarctic
- 1215 Peninsula, Scientific Reports, 15, 10038, 10.1038/s41598-025-92914-9, 2025.
- 1216 Jabre, L., and Bertrand, E. M.: Interactive effects of iron and temperature on the growth of
- 1217 Fragilariopsis cylindrus, Limnology and Oceanography Letters, 5, 363-370, 2020.
- 1218 Johnsen, G., Dalløkken, R., Eikrem, W., Legrand, C., Aure, J., and Skjoldal, H. R.: ECO-
- 1219 PHYSIOLOGY, BIO-OPTICS AND TOXICITY OF THE ICHTHYOTOXIC CHRYSOCHROMULINA
- 1220 LEADBEATERI (PRYMNESIOPHYCEAE), Journal of Phycology, 35, 1465-1476,
- 1221 https://doi.org/10.1046/j.1529-8817.1999.3561465.x, 1999.
- 1222 Jones, M. E., Bromwich, D. H., Nicolas, J. P., Carrasco, J., Plavcová, E., Zou, X., and Wang,
- 1223 S.-H.: Sixty years of widespread warming in the southern middle and high latitudes (1957–
- 1224 2016), Journal of Climate, 32, 6875-6898, 2019.
- 1225 Kahru, M., Mitchell, B. G., Gille, S. T., Hewes, C. D., and Holm-Hansen, O.: Eddies enhance
- 1226 biological production in the Weddell-Scotia Confluence of the Southern Ocean,
- 1227 Geophysical Research Letters, 34, https://doi.org/10.1029/2007GL030430, 2007.
- 1228 Kang, J.-S., Kang, S.-H., Kim, D., and Kim, D.-Y.: Planktonic centric diatom Minidiscus
- 1229 chilensis dominated sediment trap material in eastern Bransfield Strait, Antarctica, Marine
- 1230 Ecology Progress Series, 255, 93-99, 2003.
- 1231 Kang, S.-H., and Fryxell, G. A.: Fragilariopsis cylindrus (Grunow) Krieger: The most
- 1232 abundant diatom in water column assemblages of Antarctic marginal ice-edge zones,
- 1233 Polar Biol, 12, 609-627, 10.1007/BF00236984, 1992.
- 1234 Kang, S. H., and Fryxell, G. A.: Phytoplankton in the Weddell Sea, Antarctica: composition,
- 1235 abundance and distribution in water-column assemblages of the marginal ice-edge zone
- 1236 during austral autumn, Marine Biology, 116, 335-348, 10.1007/BF00350024, 1993.
- 1237 Kang, S. H., and Lee, S. H.: Antarctic phytoplankton assemblage in the western Bransfield
- 1238 Strait region, February 1993: composition, biomass, and mesoscale distributions, Marine
- 1239 Ecology Progress Series, 129, 253-267, 1995.
- 1240 Karl, D. M., Tilbrook, B. D., and Tien, G.: Seasonal coupling of organic matter production
- 1241 and particle flux in the western Bransfield Strait, Antartica, Deep Sea Research Part A.
- 1242 Oceanographic Research Papers, 38, 1097-1126, https://doi.org/10.1016/0198-
- 1243 <u>0149(91)90098-Z</u>, 1991.
- 1244 Klunder, M. B., Laan, P., De Baar, H. J. W., Middag, R., Neven, I., and Van Ooijen, J.:
- 1245 Dissolved Fe across the Weddell Sea and Drake Passage: impact of DFe on nutrient
- 1246 uptake, Biogeosciences, 11, 651-669, 10.5194/bg-11-651-2014, 2014.

- 1247 Kuwata, A., and Takahashi, M.: Life-form population responses of a marine planktonic
- 1248 diatom, Chaetoceros pseudocurvisetus, to oligotrophication in regionally upwelled water,
- 1249 Marine Biology, 107, 503-512, 1990.
- Landry, M. R., Selph, K. E., Brown, S. L., Abbott, M. R., Measures, C. I., Vink, S., Allen, C. B.,
- 1251 Calbet, A., Christensen, S., and Nolla, H.: Seasonal dynamics of phytoplankton in the
- 1252 Antarctic Polar Front region at 170° W, Deep Sea Research Part II: Topical Studies in
- 1253 Oceanography, 49, 1843-1865, 2002.
- 1254 Landry, M. R., Freibott, A. L., Stukel, M. R., Selph, K. E., Allen, A. E., and Rabines, A.:
- 1255 Phytoplankton growth and grazing dynamics during anomalous heat wave and suppressed
- 1256 upwelling conditions in the southern California Current, Deep Sea Research Part I:
- 1257 Oceanographic Research Papers, 210, 104353, 2024.
- 1258 Lange, C. B., Treppke, U. F., and Fischer, G.: Seasonal diatom fluxes in the Guinea Basin
- 1259 and their relationships to trade winds, hydrography and upwelling events, Deep Sea
- 1260 Research Part I: Oceanographic Research Papers, 41, 859-878, 1994.
- 1261 Latorre, M. P., Iachetti, C. M., Schloss, I. R., Antoni, J., Malits, A., de la Rosa, F., De Troch,
- 1262 M., Garcia, M. D., Flores-Melo, X., and Romero, S. I.: Summer heatwaves affect coastal
- 1263 Antarctic plankton metabolism and community structure, Journal of Experimental Marine
- 1264 Biology and Ecology, 567, 151926, 2023.
- 1265 Leblanc, K., Arístegui, J., Kopczynska, E., Marshall, H., Peloquin, J., Piontkovski, S.,
- 1266 Poulton, A., Quéguiner, B., Schiebel, R., and Shipe, R.: A global diatom database-
- abundance, biovolume and biomass in the world ocean, 2012.
- 1268 Leblanc, K., Quéguiner, B., Diaz, F., Cornet, V., Michel-Rodriguez, M., Durrieu de Madron,
- 1269 X., Bowler, C., Malviya, S., Thyssen, M., Grégori, G., Rembauville, M., Grosso, O., Poulain,
- 1270 J., de Vargas, C., Pujo-Pay, M., and Conan, P.: Nanoplanktonic diatoms are globally
- 1271 overlooked but play a role in spring blooms and carbon export, Nature Communications,
- 1272 9, 953, 10.1038/s41467-018-03376-9, 2018.
- 1273 Lee, H., Calvin, K., Dasgupta, D., Krinner, G., Mukherji, A., Thorne, P., Trisos, C., Romero, J.,
- 1274 Aldunce, P., and Barrett, K.: Climate change 2023: synthesis report. Contribution of
- working groups I, II and III to the sixth assessment report of the intergovernmental panel on
- 1276 climate change, 2023.
- Legendre, L., and Le Fèvre, J.: Microbial food webs and the export of biogenic carbon in
- 1278 oceans, Aquatic Microbial Ecology, 9, 69-77, 1995.
- 1279 Leventer, A.: Sediment trap diatom assemblages from the northern Antarctic Peninsula
- region, Deep Sea Research Part A. Oceanographic Research Papers, 38, 1127-1143,
- 1281 http://dx.doi.org/10.1016/0198-0149(91)90099-2, 1991.
- 1282 Leventer, A.: Modern distribution of diatoms in sediments from the George V Coast,
- 1283 Antarctica, Marine Micropaleontology, 19, 315-332, 1992.
- 1284 Lundholm, N., and Hasle, G. R.: Are Fragilariopsis cylindrus and Fragilariopsis nana
- 1285 bipolar diatoms?–Morphological and molecular analyses of two sympatric species, Nova
- 1286 Hedwigia, Beiheft, 133, 231-250, 2008.
- 1287 Majewska, R., Kuklinski, P., Balazy, P., Yokoya, N. S., Paternostro Martins, A., and De
- 1288 Stefano, M.: A comparison of epiphytic diatom communities on Plocamium cartilagineum
- 1289 (Plocamiales, Florideophyceae) from two Antarctic areas, Polar Biol, 38, 189-205,
- 1290 10.1007/s00300-014-1578-7, 2015.
- 1291 Malinverno, E., Triantaphyllou, M. V., and Dimiza, M. D.: Coccolithophore assemblage
- 1292 distribution along a temperate to polar gradient in the West Pacific sector of the Southern
- 1293 Ocean (January 2005), Micropaleontology, 61, 489–506, 2015.
- Martin, J. H., Fitzwater, S. E., and Gordon, R. M.: Iron deficiency limits phytoplankton
- 1295 growth in Antarctic waters, Global Biogeochemical Cycles, 4, 5-12,
- 1296 doi:10.1029/GB004i001p00005, 1990.
- 1297 Martínez, J., Leonelli, F. E., García-Ladona, E., Garrabou, J., Kersting, D. K., Bensoussan,
- 1298 N., and Pisano, A.: Evolution of marine heatwaves in warming seas: the Mediterranean Sea

- 1299 case study, Frontiers in Marine Science, Volume 10 2023, 10.3389/fmars.2023.1193164,
- 1300 2023.
- 1301 Merchant, C. J., Embury, O., Bulgin, C. E., Block, T., Corlett, G. K., Fiedler, E., Good, S. A.,
- 1302 Mittaz, J., Rayner, N. A., and Berry, D.: Satellite-based time-series of sea-surface
- temperature since 1981 for climate applications, Scientific data, 6, 223, 2019.
- 1304 Meredith, M. P., and Hogg, A. M.: Circumpolar response of Southern Ocean eddy activity to
- 1305 a change in the Southern Annular Mode, Geophysical Research Letters, 33,
- 1306 https://doi.org/10.1029/2006GL026499, 2006.
- 1307 Meredith, M. P., Woodworth, P. L., Chereskin, T. K., Marshall, D. P., Allison, L. C., Bigg, G.
- 1308 R., Donohue, K., Heywood, K. J., Hughes, C. W., and Hibbert, A.: Sustained monitoring of
- 1309 the Southern Ocean at Drake Passage: Past achievements and future priorities, Reviews of
- 1310 Geophysics, 49, 2011.
- 1311 Meredith, M. P., Falk, U., Bers, A. V., Mackensen, A., Schloss, I. R., Ruiz Barlett, E., Jerosch,
- 1312 K., Silva Busso, A., and Abele, D.: Anatomy of a glacial meltwater discharge event in an
- 1313 Antarctic cove, Philosophical Transactions of the Royal Society A: Mathematical, Physical
- 1314 and Engineering Sciences, 376, 20170163, 2018.
- 1315 Moline, M. A., Claustre, H., Frazer, T. K., Schofield, O., and Vernet, M.: Alteration of the
- 1316 food web along the Antarctic Peninsula in response to a regional warming trend, Global
- 1317 Change Biology, 10, 1973-1980, 2004.
- 1318 Moline, M. A., Karnovsky, N. J., Brown, Z., Divoky, G. J., Frazer, T. K., Jacoby, C. A., Torres, J.
- 1319 J., and Fraser, W. R.: High latitude changes in ice dynamics and their impact on polar
- marine ecosystems, Annals of the New York Academy of Sciences, 1134, 267, 2008.
- Montes-Hugo, M., Vernet, M., Martinson, D., Smith, R., and Iannuzzi, R.: Variability on
- 1322 phytoplankton size structure in the western Antarctic Peninsula (1997–2006), Deep Sea
- 1323 Research Part II: Topical Studies in Oceanography, 55, 2106-2117, 2008.
- Montie, S., Thomsen, M. S., Rack, W., and Broady, P. A.: Extreme summer marine
- heatwaves increase chlorophyll a in the Southern Ocean, Antarctic Science, 32, 508-509,
- 1326 10.1017/S0954102020000401, 2020.
- Oh, J.-H., Noh, K. M., Lim, H.-G., Jin, E. K., Jun, S.-Y., and Kug, J.-S.: Antarctic meltwater-
- 1328 induced dynamical changes in phytoplankton in the Southern Ocean, Environmental
- 1329 Research Letters, 17, 024022, 10.1088/1748-9326/ac444e, 2022.
- 1330 Olguin, H. F., Boltovskoy, D., Lange, C. B., and Brandini, F.: Distribution of spring
- 1331 phytoplankton (mainly diatoms) in the upper 50 m of the Southwestern Atlantic Ocean
- 1332 (30–61 S), Journal of plankton research, 28, 1107-1128, 2006.
- Oliver, E. C., Donat, M. G., Burrows, M. T., Moore, P. J., Smale, D. A., Alexander, L. V.,
- 1334 Benthuysen, J. A., Feng, M., Sen Gupta, A., and Hobday, A. J.: Longer and more frequent
- marine heatwaves over the past century, Nature communications, 9, 1-12, 2018.
- Oliver, E. C. J., Benthuysen, J. A., Darmaraki, S., Donat, M. G., Hobday, A. J., Holbrook, N.
- 1337 J., Schlegel, R. W., and Sen Gupta, A.: Marine Heatwaves, Annual Review of Marine
- 1338 Science, 13, 313-342, https://doi.org/10.1146/annurev-marine-032720-095144, 2021.
- 1339 Orsi, A. H., Whitworth Iii, T., and Nowlin Jr, W. D.: On the meridional extent and fronts of
- 1340 the Antarctic Circumpolar Current, Deep Sea Research Part I: Oceanographic Research
- 1341 Papers, 42, 641-673, http://dx.doi.org/10.1016/0967-0637(95)00021-W, 1995.
- 1342 Patil, S. M., Mohan, R., Shetye, S. S., Gazi, S., Baumann, K.-H., and Jafar, S.: Biogeographic
- 1343 distribution of extant Coccolithophores in the Indian sector of the Southern Ocean, Marine
- 1344 Micropaleontology, 137, 16-30, https://doi.org/10.1016/j.marmicro.2017.08.002, 2017.
- Pauli, N.-C., Flintrop, C. M., Konrad, C., Pakhomov, E. A., Swoboda, S., Koch, F., Wang, X.-
- 1346 L., Zhang, J.-C., Brierley, A. S., Bernasconi, M., Meyer, B., and Iversen, M. H.: Krill and salp
- 1347 faecal pellets contribute equally to the carbon flux at the Antarctic Peninsula, Nature
- 1348 Communications, 12, 7168, 10.1038/s41467-021-27436-9, 2021.

- 1349 Peck, L. S., Barnes, D. K. A., Cook, A. J., Fleming, A. H., and Clarke, A.: Negative feedback
- in the cold: ice retreat produces new carbon sinks in Antarctica, Global Change Biology,
- 1351 16, 2614-2623, https://doi.org/10.1111/j.1365-2486.2009.02071.x, 2010.
- 1352 Peña, M. A., Nemcek, N., and Robert, M.: Phytoplankton responses to the 2014–2016
- 1353 warming anomaly in the northeast subarctic Pacific Ocean, Limnology and Oceanography,
- 1354 64, 515-525, https://doi.org/10.1002/lno.11056, 2019.
- 1355 Plum, C., Hillebrand, H., and Moorthi, S.: Krill vs salps: dominance shift from krill to salps
- 1356 is associated with higher dissolved N:P ratios, Scientific Reports, 10, 5911,
- 1357 10.1038/s41598-020-62829-8, 2020.
- 1358 Rembauville, M., Manno, C., Tarling, G. A., Blain, S., and Salter, I.: Strong contribution of
- 1359 diatom resting spores to deep-sea carbon transfer in naturally iron-fertilized waters
- downstream of South Georgia, Deep Sea Research Part I: Oceanographic Research
- 1361 Papers, 115, 22-35, http://doi.org/10.1016/j.dsr.2016.05.002, 2016.
- 1362 Rembauville, M., Blain, S., Manno, C., Tarling, G., Thompson, A., Wolff, G., and Salter, I.:
- 1363 The role of diatom resting spores in pelagic-benthic coupling in the Southern Ocean,
- 1364 2018.
- 1365 Rigual-Hernández, A. S., Trull, T. W., Bray, S. G., Closset, I., and Armand, L. K.: Seasonal
- 1366 dynamics in diatom and particulate export fluxes to the deep sea in the Australian sector
- of the southern Antarctic Zone, Journal of Marine Systems, 142, 62-74,
- 1368 http://dx.doi.org/10.1016/j.jmarsys.2014.10.002, 2015.
- 1369 Rigual-Hernández, A. S., Trull, T. W., Bray, S. G., and Armand, L. K.: The fate of diatom
- 1370 valves in the Subantarctic and Polar Frontal Zones of the Southern Ocean: Sediment trap
- 1371 versus surface sediment assemblages, Palaeogeography, Palaeoclimatology,
- 1372 Palaeoecology, 457, 129-143, http://dx.doi.org/10.1016/j.palaeo.2016.06.004, 2016.
- 1373 Rigual-Hernández, A. S., Trull, T. W., Flores, J. A., Nodder, S. D., Eriksen, R., Davies, D. M.,
- Hallegraeff, G. M., Sierro, F. J., Patil, S. M., Cortina, A., Ballegeer, A. M., Northcote, L. C.,
- 1375 Abrantes, F., and Rufino, M. M.: Full annual monitoring of Subantarctic Emiliania huxleyi
- 1376 populations reveals highly calcified morphotypes in high-CO2 winter conditions, Scientific
- 1377 Reports, 10, 2594, 10.1038/s41598-020-59375-8, 2020a.
- 1378 Rigual-Hernández, A. S., Trull, T. W., Nodder, S. D., Flores, J. A., Bostock, H., Abrantes, F.,
- 1379 Eriksen, R. S., Sierro, F. J., Davies, D. M., Ballegeer, A. M., Fuertes, M. A., and Northcote, L.
- 1380 C.: Coccolithophore biodiversity controls carbonate export in the Southern Ocean,
- 1381 Biogeosciences, 17, 245-263, 10.5194/bg-17-245-2020, 2020b.
- 1382 Rigual Hernández, A. S., Flores, J. A., Sierro, F. J., Fuertes, M. A., Cros, L., and Trull, T. W.:
- 1383 Coccolithophore populations and their contribution to carbonate export during an annual
- cycle in the Australian sector of the Antarctic zone, Biogeosciences, 15, 1843-1862,
- 1385 10.5194/bg-15-1843-2018, 2018.
- 1386 Rintoul, S. R., Donguy, J. R., and Roemmich, D. H.: Seasonal evolution of upper ocean
- 1387 thermal structure between Tasmania and Antarctica, Deep Sea Research Part I:
- 1388 Oceanographic Research Papers, 44, 1185-1202, http://dx.doi.org/10.1016/S0967-
- 1389 <u>0637(96)00125-2</u>, 1997.
- 1390 Rintoul, S. R., and Sokolov, S.: Baroclinic transport variability of the Antarctic Circumpolar
- 1391 Current south of Australia, J. Geophys. Res, 106, 2815-2832, 2001.
- 1392 Rintoul, S. R., Chown, S. L., DeConto, R. M., England, M. H., Fricker, H. A., Masson-
- 1393 Delmotte, V., Naish, T. R., Siegert, M. J., and Xavier, J. C.: Choosing the future of Antarctica,
- 1394 Nature, 558, 233-241, 10.1038/s41586-018-0173-4, 2018.
- 1395 Rivero-Calle, S., Gnanadesikan, A., Del Castillo, C. E., Balch, W. M., and Guikema, S. D.:
- 1396 Multidecadal increase in North Atlantic coccolithophores and the potential role of rising
- 1397 CO2, Science, 350, 1533-1537, 10.1126/science.aaa8026, 2015.
- 1398 Saavedra-Pellitero, M., and Baumann, K.-H.: Comparison of living and surface sediment
- 1399 coccolithophore assemblages in the Pacific sector of the Southern Ocean,
- 1400 Micropaleontology, 61, 507-520, 2015.

- 1401 Saavedra-Pellitero, M., Baumann, K. H., Fuertes, M. Á., Schulz, H., Marcon, Y., Vollmar, N.
- 1402 M., Flores, J. A., and Lamy, F.: Calcification and latitudinal distribution of extant
- 1403 coccolithophores across the Drake Passage during late austral summer 2016,
- 1404 Biogeosciences, 16, 3679-3702, 10.5194/bg-16-3679-2019, 2019.
- 1405 Schlitzer, R.: Ocean Data View, https://odv.awi.de, 2021.
- 1406 Scott, F. J., and Marchant, H. J.: Antarctic marine protists, 2005.
- 1407 Servettaz, A. P. M., Isaji, Y., Yoshikawa, C., Jang, Y., Khim, B. K., Ryu, Y., Sigman, D. M.,
- 1408 Ogawa, N. O., Jiménez-Espejo, F. J., and Ohkouchi, N.: Sea ice and mixed layer depth
- 1409 influence on nitrate depletion and associated isotopic effects in the Drake Passage-
- 1410 Weddell Sea region, Southern Ocean, Biogeosciences, 22, 2239-2260, 10.5194/bg-22-
- 1411 2239-2025, 2025.
- 1412 Silva, J. F. d., Oliveira, M. A., Paidano Alves, R., Vestena Cassol, A. P., Ribeiro da
- 1413 Anunciação, R., Pereira da Silva, E., Schünemann, A. L., and Batista Pereira, A.:
- 1414 Geographic distribution of epilithic diatoms (Bacillariophyceae) in Antarctic lakes,
- 1415 South Shetland Islands, Maritime Antarctica Region, Check List, 15, 797-809, 2019.
- 1416 Smetacek, V., Assmy, P., and Henjes, J.: The role of grazing in structuring Southern Ocean
- pelagic ecosystems and biogeochemical cycles, Antarctic Science, 16, 541-558,
- 1418 doi:10.1017/S0954102004002317, 2004.
- 1419 Smith, K. E., Burrows, M. T., Hobday, A. J., King, N. G., Moore, P. J., Sen Gupta, A.,
- 1420 Thomsen, M. S., Wernberg, T., and Smale, D. A.: Biological impacts of marine heatwaves,
- 1421 Annual review of marine science, 15, 119-145, 2023.
- 1422 Suryawanshi, K., Jena, B., Bajish, C., and Anilkumar, N.: Recent decline in Antarctic sea
- 1423 ice cover from 2016 to 2022: insights from satellite observations, argo floats, and model
- reanalysis, Tellus A: Dynamic Meteorology and Oceanography, 75, 2023.
- 1425 Team, R. C.: R: A language and environment for statistical computing, R foundation for
- 1426 statistical computing, Vienna, Austria, 2021.
- 1427 ter Braak, C. J. F., and Verdonschot, P. F. M.: Canonical correspondence analysis and
- 1428 related multivariate methods in aquatic ecology, Aquatic Sciences, 57, 255-289,
- 1429 10.1007/bf00877430, 1995.
- 1430 Tetzner, D., Thomas, E., and Allen, C.: A validation of ERA5 reanalysis data in the Southern
- 1431 Antarctic Peninsula—Ellsworth land region, and its implications for ice core studies,
- 1432 Geosciences, 9, 289, 2019.
- 1433 Thomalla, S. J., Nicholson, S.-A., Ryan-Keogh, T. J., and Smith, M. E.: Widespread changes
- in Southern Ocean phytoplankton blooms linked to climate drivers, Nature Climate
- 1435 Change, 13, 975-984, 10.1038/s41558-023-01768-4, 2023.
- 1436 Toggweiler, J., and Samuels, B.: Effect of Drake Passage on the global thermohaline
- 1437 circulation, Deep Sea Research Part I: Oceanographic Research Papers, 42, 477-500,
- 1438 1995
- 1439 Treppke, U. F., Lange, C. B., and Wefer, G.: Vertical fuxes of diatoms and silicofagellates in
- 1440 the eastern equatorial Atlantic, and their contribution to the sedimentary record, Marine
- 1441 Micropaleontology, 28, 73-96, 1996.
- 1442 Trull, T. W., Passmore, A., Davies, D. M., Smit, T., Berry, K., and Tilbrook, B.: Distribution of
- 1443 planktonic biogenic carbonate organisms in the Southern Ocean south of Australia: a
- baseline for ocean acidification impact assessment, Biogeosciences, 15, 31-49, 2018.
- Turner, J., Lu, H., King, J., Marshall, G. J., Phillips, T., Bannister, D., and Colwell, S.: Extreme
- temperatures in the Antarctic, Journal of Climate, 34, 2653-2668, 2021.
- 1447 Vaughan, D. G., Marshall, G. J., Connolley, W. M., Parkinson, C., Mulvaney, R., Hodgson, D.
- 1448 A., King, J. C., Pudsey, C. J., and Turner, J.: Recent Rapid Regional Climate Warming on the
- 1449 Antarctic Peninsula, Climatic Change, 60, 243-274, 10.1023/A:1026021217991, 2003.
- 1450 Venables, H., and Moore, C. M.: Phytoplankton and light limitation in the Southern Ocean:
- 1451 Learning from high-nutrient, high-chlorophyll areas, Journal of Geophysical Research:
- 1452 Oceans, 115, C02015, 10.1029/2009JC005361, 2010.

- 1453 Vernet, M., Smith Jr, K. L., Cefarelli, A. O., Helly, J. J., Kaufmann, R. S., Lin, H., Long, D. G.,
- 1454 Murray, A. E., Robison, B. H., and Ruhl, H. A.: Islands of ice: Influence of free-drifting
- 1455 Antarctic icebergs on pelagic marine ecosystems, Oceanography, 25, 2012.
- 1456 Villafañe, V. E., Helbling, E. W., and Holm-Hansen, O.: Spatial and temporal variability of
- 1457 phytoplankton biomass and taxonomic composition around Elephant Island, Antarctica,
- 1458 during the summers of 1990–1993, Marine Biology, 123, 677-686, 10.1007/bf00349110,
- 1459 1995.
- 1460 Wernberg, T., Smale, D. A., Tuya, F., Thomsen, M. S., Langlois, T. J., de Bettignies, T.,
- 1461 Bennett, S., and Rousseaux, C. S.: An extreme climatic event alters marine ecosystem
- structure in a global biodiversity hotspot, Nature Climate Change, 3, 78-82,
- 1463 10.1038/nclimate1627, 2013.
- 1464 Wernberg, T., Bennett, S., Babcock, R. C., de Bettignies, T., Cure, K., Depczynski, M.,
- 1465 Dufois, F., Fromont, J., Fulton, C. J., Hovey, R. K., Harvey, E. S., Holmes, T. H., Kendrick, G.
- 1466 A., Radford, B., Santana-Garcon, J., Saunders, B. J., Smale, D. A., Thomsen, M. S., Tuckett,
- 1467 C. A., Tuya, F., Vanderklift, M. A., and Wilson, S.: Climate-driven regime shift of a
- temperate marine ecosystem, Science, 353, 169-172, doi:10.1126/science.aad8745,
- 1469 2016.
- 1470 Wilks, J. V., Nodder, S. D., and Rigual-Hernández, A.: Diatom and coccolithophore species
- 1471 fluxes in the Subtropical Frontal Zone, east of New Zealand, Deep Sea Research Part I:
- 1472 Oceanographic Research Papers, 169, 103455, https://doi.org/10.1016/j.dsr.2020.103455,
- 1473 2021.

- 1474 Wright, S. W., van den Enden, R. L., Pearce, I., Davidson, A. T., Scott, F. J., and Westwood,
- 1475 K. J.: Phytoplankton community structure and stocks in the Southern Ocean (30–80 E)
- 1476 determined by CHEMTAX analysis of HPLC pigment signatures, Deep Sea Research Part II:
- 1477 Topical Studies in Oceanography, 57, 758-778, 2010.
- 1478 Young, J., Geisen, M., Cross, L., Kleijne, A., Sprengel, C., Probert, I., and Østergaard, J.: A
- 1479 guide to extant coccolithophore taxonomy, Journal of Nanoplankton Research Special
- 1480 Issue 1, International Nannoplankton Association, 2003.
- Nannotax3 website: http://www.mikrotax.org/Nannotax3 access: July 2021, 2024.
- 1482 Zhu, J., Xie, A., Qin, X., Wang, Y., Xu, B., and Wang, Y.: An assessment of ERA5 reanalysis
- 1483 for Antarctic near-surface air temperature, Atmosphere, 12, 217, 2021.
- 1484 Zielinski, U., and Gersonde, R.: Diatom distribution in Southern Ocean surface sediments
- 1485 (Atlantic sector): Implications for paleoenvironmental reconstructions, Palaeogeography,
- 1486 Palaeoclimatology, Palaeoecology, 129, 213-250, http://dx.doi.org/10.1016/S0031-
- 1487 <u>0182(96)00130-7</u>, 1997.